

Inverse mass cascade in dark matter flow and effects on halo mass functions

Zhijie (Jay) Xu,¹★

¹*Physical and Computational Sciences Directorate, Pacific Northwest National Laboratory; Richland, WA 99352, USA*

Accepted XXX. Received YYY; in original form ZZZ

ABSTRACT

The inverse mass cascade is a key feature of statistically steady state for self-gravitating collisionless dark matter flow (SG-CFD). The continuous mass transfer from small to large mass scales (inverse cascade) is formulated. Direct effect of mass cascade on halo mass function is discussed. Mass cascade is local, two-way, and asymmetric in mass space. Halos inherit/pass their mass from/to halos of similar size. Two distinct ranges are identified: a propagation range with scale-independent rate of mass transfer and a deposition range with cascaded mass consumed to grow halos. Simple dimensional analysis leads to a power-law mass function in propagation range with a geometry exponent λ . A fundamental merging frequency $f_0 \sim m_p^{\lambda-1} a^{-1}$ is identified, where a is scale factor. The particle mass m_p can be determined if that frequency is known. The rate of mass transfer $\epsilon_m \sim a^{-1}$ is independent of halo mass, a key feature of propagation range. Typical halos grow as $m_h \sim a^{3/2}$ and waiting time or halo lifespan scales as $\sim m_h^{-\lambda}$. Chain reaction of mass cascade provides non-equilibrium system (dark matter flow) a mechanism to continuously release energy and maximize entropy. A continuous injection of mass ("free radicals") at the smallest scale is required to sustain the everlasting inverse mass cascade such that total halo mass M_h increases as $a^{1/2}$. These "radicals" might be directly generated at the smallest Planck scale or by a direct cascade from large to small scales. Entire mass cascade can be formulated by random walk in mass space, where halos migrate with an exponential distribution of waiting time. This results in a heterogeneous diffusion model, where Press-Schechter mass function can be fully derived without relying on any specific collapse models. A double- λ mass function is proposed with different λ for two ranges and agrees with N-body simulations.

Key words: Dark matter; N-body simulations; Theoretical models

CONTENTS

- 1 Introduction
- 2 N-body simulations and numerical data
- 3 Real-scape inverse mass cascade in SG-CFD
 - 3.1 Mass redistribution among halo groups
 - 3.2 Time and mass scales in inverse mass cascade
- 4 Formulating inverse mass cascade
 - 4.1 Mass flux and mass transfer functions
 - 4.2 Chain reaction and random walk for inverse mass cascade
 - 4.3 Heterogeneous diffusion model and halo mass functions
- 5 Connections to halo mass functions
 - 5.1 Existing halo mass functions
 - 5.2 Double- λ halo mass function
- 6 Conclusions

1 INTRODUCTION

Collisionless systems often have properties suggesting common physical principles that control their motion and evolution. The self-gravitating collisionless fluid dynamics (SG-CFD) is the study of

motion of collisionless matter due to the influence of its own gravity. Typical examples can be the large-scale gravitational collapse of collisionless dark matter, which is essentially a nonlinear self-gravitating collisionless flow problem (Lukic et al. 2007). Gravitational instability leads to the self-organization of collisionless dark matter particles and the formation and evolution of large-scale structures. Within a CDM paradigm (Blumenthal et al. 1984), the initial density fluctuation has a larger amplitude at smaller scales. The formation of structures starts from the gravitational collapse of small-scale density fluctuations and proceeds hierarchically such that small structures coalesce into large structures in a "bottom-up" fashion. Highly localized, over-dense, and virialized structure (halo) is a major manifestation of the nonlinear gravitational collapse (Neyman & Scott 1952; Cooray & Sheth 2002) and the building blocks of large-scale structures, whose abundance and internal structures have been extensively studied over the last several decades.

The abundance of halos is described by a halo mass function, one of the most fundamental quantities to probe the large-scale structures and model the structure formation and evolution. The first landmark might be the Press-Schechter (PS) formalism (Press & Schechter 1974; Bond et al. 1991), which allows one to predict the shape and evolution of mass function. The distribution of halo mass is determined by postulating that the probability of forming halos is related to the amplitude of density fluctuations on that scale. Halos will form at some mass scale once the smoothed linear density contrast

★ E-mail: zhijie.xu@pnnl.gov; zhijie.xu@hotmail.com

on that scale exceeds a threshold value δ_c . This threshold value must be analytically derived by examining the nonlinear collapse of a spherical top hat over-density (Tomita 1969; Gunn & Gott 1972). Although mathematically less rigorous, PS formalism and its extensions are very useful and allow one to compute many different structural properties. Examples are the halo mass function, merging rates, and clustering properties. This paper will attempt to explore the halo mass function from a completely different perspective via the mass cascade between halos on different mass scales.

In contrast to the self-gravitating collisionless dark matter flow, the incompressible collisional hydrodynamics with a high Reynolds number also develops instability that initiates the hydrodynamic turbulence. Turbulence consists of a random collection of eddies (building blocks) at different length scales that are interacting with each other and dynamically changing in space and time. This suggests that we should revisit some fundamental ideas of hydrodynamic turbulence, a long-standing and probably the last unresolved problem in classical physics. The story began with a famous poem by Richardson in the 1920s (Richardson 1922):

"Big whirls have little whirls, That feed on their velocity;
And little whirls have lesser whirls, And so on to viscosity."

The poem describes a conceptual picture that large eddies feed smaller eddies, which feed even smaller eddies, and then lead to viscous dissipation at the smallest scale, i.e. the concept of a direct energy cascade (see Fig. 1). There is a broad spectrum of eddy sizes within fully developed turbulence. Large eddies are usually created by the instability of large scale mean flow at integral scale L and rapidly break up and pass their kinetic energy to smaller eddies due to inertial force. Smaller eddies are transient and in turn, pass their energy to even smaller eddies. The cascade continues down the scale and stops to operate at the smallest eddies (dissipation scale η) where the viscous force becomes dominant over the inertial force.

Provided the Reynolds number is high enough, there exists a range of length scales where the viscous force is negligible and inertial force is dominant. The rate ϵ of energy passing down the cascade should be scale-independent in this range and match exactly the rate of energy dissipation at the smallest scale. While the direct energy cascade is a dominant feature for three-dimensional turbulence, the existence of a range of scales over which kinetic energy is transferred from small to large scales, i.e. an inverse energy cascade, was predicted in the late 1960s for two-dimensional turbulence (Kraichnan 1967). A potential mechanism for inverse energy cascade can be the vortex merger. Eddies are generated at small scales (the energy injection scale) and cluster and merge into larger eddies, which in turn merge into even larger eddies with kinetic energy continuously transferred from small to large length scales.

While "eddy" itself is not a well-defined object in the turbulence literature, a striking similarity can be identified between the self-gravitating collisionless dark matter flow (SG-CFD) and the two-dimensional turbulence when "eddy" (or "whirls") is simply replaced by "halos" in the poem (Fig. 1):

"Little halos have big halos, That feed on their mass;
And big halos have greater halos, And so on to growth."

This conceptual picture describes the inverse mass cascade of SG-CFD as follows: there exists a broad spectrum of halo sizes. Small halos are created by gravitational instability at the smallest mass scale and interacting and merging with other halos. Halos pass their mass onto larger and larger halos (propagation range), until halo mass

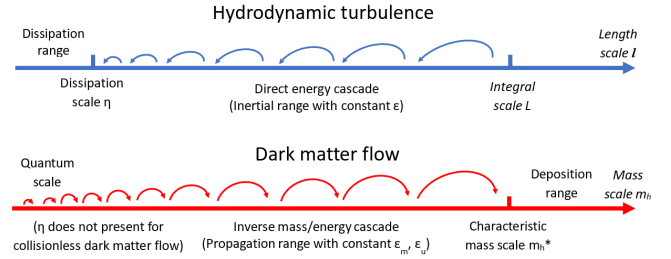


Figure 1. Schematic plot of direct energy cascade in hydrodynamic turbulence that is mediated by eddies of different scales. By contrast, halos of different sizes facilitate the inverse mass/energy cascade in dark matter flow. Relevant time and mass scales in dark matter flow are presented in Section 3.2.

growth becomes dominant over mass propagation (deposition range with $m_h > m_h^*$). Consequently, we expect a continuous cascade of mass from small to the large mass scales and a scale-independent rate of mass transfer ϵ_m and rate of energy transfer ϵ_u in certain range of mass scales (mass propagation range). The everlasting inverse mass cascade is a distinct feature of the statistically steady state of dark matter flow and requires continuous mass generation at the smallest scale with the same rate as mass propagation. Finally, strong similarity with two-dimensional turbulence prompts us to revisit and formulate inverse mass cascade in SG-CFD to explore new discoveries and insights.

This paper will develop the idea of inverse mass cascade into rigorous mathematical formulations. We expect two important aspects of gravitational collapse, i.e. the abundance and internal structure of halos, are highly correlated with inverse mass cascade. Despite the path already explored by many pioneers, we are particularly interested in the direct effects of mass cascade and its connections with halo abundance (this work), halo properties and internal structures (Xu 2021a, 2022e), energy cascade (Xu 2021e), maximum entropy distributions (Xu 2021b), and momentum and energy evolution (Xu 2022h). The mass and energy cascades will also facilitate the development of statistical theory for dark matter flow (Xu 2022f,g,i) with potential relevance to dark matter particle mass and properties (Xu 2022j), MOND (modified Newtonian dynamics) theory (Xu 2022k), and baryonic-to-halo mass relation (Xu 2022l).

The rest of paper is organized as follows: Section 2 introduces the simulation and numerical data used for this work, followed by the concept of inverse mass cascade and the associated time/mass scales in Section 3. The formulation for inverse mass cascade in different ranges is presented in Section 4. Its connections to halo abundance are presented in Sections 5, where stochastic models for halo mass function are presented with complete solutions and new mass function provided.

2 N-BODY SIMULATIONS AND NUMERICAL DATA

The numerical data for this work is publicly available and generated from N -body simulations carried out by the Virgo consortium, an international collaboration that aims to perform large N -body simulations for the formation of large-scale structures. A comprehensive description of the simulation data can be found in (Frenk et al. 2000; Jenkins et al. 1998). As a first step, the current work focus on the matter-dominated simulations with $\Omega_0 = 1$ and a standard CDM

Table 1. Numerical parameters of N-body simulation

Run	Ω_0	Λ	h	Γ	σ_8	L (Mpc/h)	N	m_p M_\odot/h	l_{soft} (Kpc/h)
SCDM1	1.0	0.0	0.5	0.5	0.51	239.5	256^3	2.27×10^{11}	36

power spectrum (SCDM). Similar analysis can be extended to other simulations with different model assumptions and parameters.

The same set of simulation data has been widely used in a number of different studies from clustering statistics (Jenkins et al. 1998) to the formation of halo clusters in large scale environments (Colberg et al. 1999), and testing models for halo abundance and mass functions (Sheth et al. 2001). The simulation includes over $N = 256^3$ particles with mass $m_p = 2.27 \times 10^{11} M_\odot/h$. The simulation box size is around 240 Mpc/h, where h is the dimensionless Hubble constant in the unit of $100 km/Mpc \cdot s$.

The friends-of-friends algorithm (FOF) was used to identify all halos from simulation data that depends only on a dimensionless parameter b , which defines the linking length $b(N/V)^{-1/3}$, where V is the volume of simulation box. Halos were identified with a linking length parameter of $b = 0.2$ in this work. All halos identified from the simulation data were first grouped into halo groups of different sizes according to halo mass m_h (or in terms of n_p , the number of particles in the halos), where $m_h = n_p m_p$. The total mass for a halo group of mass m_h is $m_g = m_h n_h$, where n_h is the number of halos in each group. Simulation results will be presented to describe the inverse mass cascade across halo groups of different mass and compared with theory. Some key parameters of N-body simulations are listed in Table 1.

Two relevant datasets from this N-body simulation, i.e. halo-based and correlation-based statistics of dark matter flow, can be found at Zenodo.org (Xu 2022a,b), along with the accompanying presentation slides, "A comparative study of dark matter flow & hydrodynamic turbulence and its applications" (Xu 2022c). All data files are also available on GitHub (Xu 2022d).

3 REAL-SPACE INVERSE MASS CASCADE IN SG-CFD

To study the mass cascade of SG-CFD, we first divide the entire system into two sub-systems: 1) out-of-halo sub-system with a total mass of M_o includes all masses that do not belong to any halos; 2) halo sub-system with a total mass of M_h includes all masses contained in all halos. The collisionless dark matter flow involves a continuous mass and energy exchange between two sub-systems. This section focuses on the real space mass cascade across halo groups at different mass scales. The real space energy cascade will be discussed in a separate paper (Xu 2021e).

3.1 Mass redistribution among halo groups

All halos in halo sub-system can be grouped into groups of halos with the same mass m_h or particle number n_p . We focus on the mass cascade between halo groups of different sizes. The starting point is to define functions describing the mass redistribution among halo groups at different redshift z . The forward mass redistribution function $D_{FM}(z_1, n_{p1}, z_2, n_{p2})$ describes the mass fraction of a halo group of size n_{p1} at redshift z_1 that is inherited from the halo group of size n_{p2} at an earlier redshift z_2 . Similarly, the backward mass redistribution function $D_{BM}(z_1, n_{p1}, z_3, n_{p3})$ can be defined as the mass fraction of a halo group of size n_{p1} at redshift z_1 that will be passed to the halo group of size n_{p3} at a later redshift z_3 .

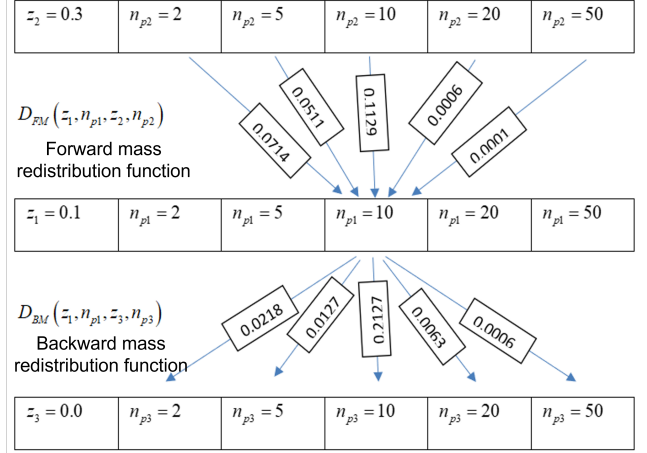


Figure 2. Example of a forward redistribution function D_{FM} from $z_2 = 0.3$ to $z_1 = 0.1$ and a backward redistribution function D_{BM} from $z_1 = 0.1$ to $z_3 = 0$ for halo group of size $n_{p1} = 10$. Figure shows the fraction of mass for a halo group of size $n_{p1} = 10$ at $z_1 = 0.1$ inherited from halo groups of different sizes at an earlier redshift $z_2 = 0.3$ (forward mass redistribution). Similarly, backward redistribution gives the fraction of mass passed to halo groups of different sizes at a later redshift $z_3 = 0$. Halo inherits and passes most of its mass from and to halos of similar size (locality in mass scale).

Figure 2 provides an example for two functions. For given z_1 , n_{p1} , and z_2 or z_3 , the normalization condition requires,

$$\sum_{n_{p2}} D_{FM}(z_1, n_{p1}, z_2, n_{p2}) = 1$$

and

$$\sum_{n_{p3}} D_{BM}(z_1, n_{p1}, z_3, n_{p3}) = 1. \quad (1)$$

For a complete picture of mass cascade among halo groups at different mass scales, Figs. 3 and 4 plot the forward and backward redistribution functions as a function of the halo group size n_{p2} or n_{p3} for five different group sizes $n_{p1} = 2, 5, 10, 20, 50$, respectively. Halo groups of five different sizes n_{p1} inherit and pass their mass to a distribution of halo group sizes. The interaction among halo groups is shown to be local in mass scale. The halo group of size n_{p1} inherits or passes most of its mass via merging/breaking between halos of similar (neighboring) size to n_{p1} and single mergers. Therefore, there are two peaks for forward/backward mass redistribution functions at around $n_{pi} \approx n_{p1}$ (halo groups of similar size) and $n_{pi} \approx 1$ (single mergers), where $i=2$ or 3 for forward or backward functions, respectively.

Groups of large halos inherit/pass their mass from/to a wider distribution of halo sizes, while groups of small halos inherit/pass their mass from/to a relatively narrower distribution of halo sizes. Both mass redistribution functions are not symmetric about the halo size n_{p1} , with more mass inherited from halo groups below the size n_{p1} and more mass passed to halo groups above the size n_{p1} .

The sharp peaks for halo groups of smaller size and the widespread distribution for halo groups of larger size in Figs. 3 and 4 indicate that small halos have relatively longer lifespan and can exist for a longer time such that most small halos will remain in the same group at a later redshift. Large halos tend to have a relatively shorter lifespan. Halo lifespan will be further discussed in Section 3.2.

To determine the direction of the mass cascade, we introduce a

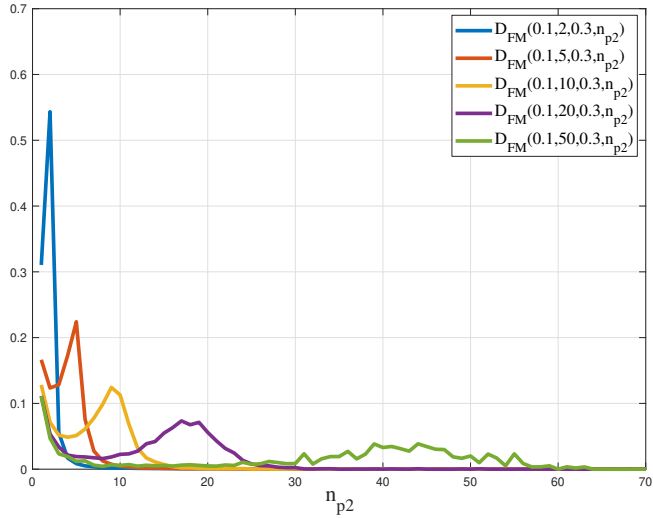


Figure 3. Forward mass redistribution function $D_{FM}(z_1, n_{p1}, z_2, n_{p2})$ from $z_2 = 0.3$ to $z_1 = 0.1$ for five different halo groups of sizes $n_{p1} = 2, 5, 10, 20, 50$, respectively. Figure shows the mass fraction of a halo group of size n_{p1} at $z_1 = 0.1$ inherited from halo groups of various sizes at an earlier redshift $z_2 = 0.3$. The interaction among groups of halos is shown to be local in the mass space, i.e. halo group of size n_{p1} inherits its mass mostly from the interaction between halo groups of similar (neighboring) sizes to n_{p1} and single mergers. Note that there are two peaks at around $n_{p2} \approx n_{p1}$ (halo groups of similar size) and $n_{p2} \approx 1$ (single merger). Halo groups of larger size inherit their mass from a wider distribution in size n_{p2} .

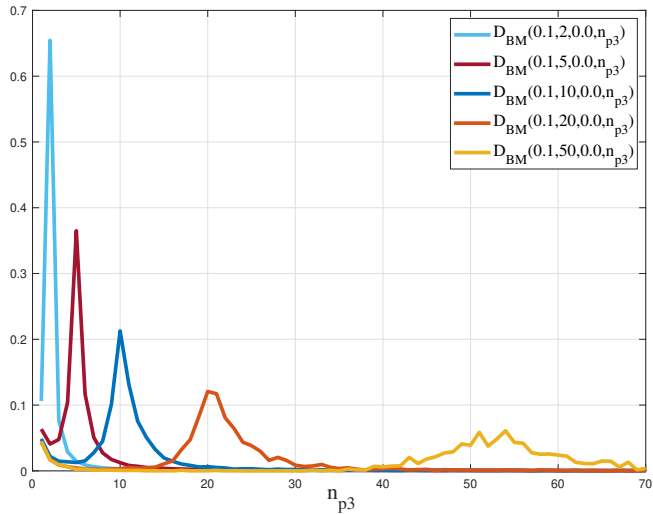


Figure 4. Backward mass redistribution function $D_{BM}(z_1, n_{p1}, z_3, n_{p3})$ from $z_1 = 0.1$ to $z_3 = 0.0$ for five different halo groups of sizes $n_{p1} = 2, 5, 10, 20, 50$, respectively. Figure shows the mass fraction of a halo group of size n_{p1} at $z_1 = 0.1$ passed to halo groups of various sizes at later redshift $z_3 = 0.0$. Again, the interaction among groups of halos is shown to be local in the mass space, i.e. halo group of size n_{p1} passes most of its mass via merging/breaking to halo groups of similar (neighboring) size to n_{p1} and single mergers. Hence, there are two peaks at around $n_{p3} \approx n_{p1}$ and $n_{p3} \approx 1$. Halo groups of larger size pass their mass to a wider distribution of halo group sizes at a later redshift, while halo groups of smaller size pass their mass to a relatively narrower distribution in size n_{p3} .

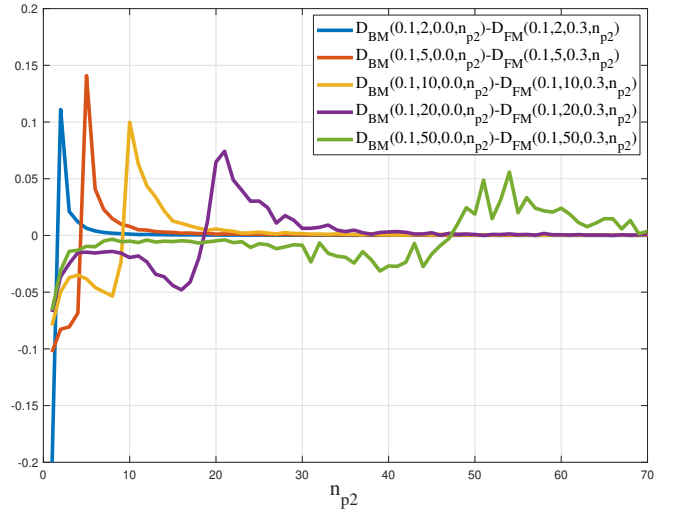


Figure 5. The net mass redistribution function D_{NM} as a function of halo group size n_{p2} for five different halo group sizes n_{p1} , with $D_{NM} < 0$ indicating that the halo group of size n_{p1} inherits more mass from the halo group of size n_{p2} than the mass it passes to the group of the same size n_{p2} . The net effect of the mass redistribution is that halos are transferring mass from smaller scales to larger scales Fig. 1, i.e. an inverse mass cascade in mass space. In contrast, direct mass cascade refers to the mass transfer from larger to smaller scales.

net mass redistribution function D_{NM} as the difference between the backward and forward mass redistribution functions,

$$D_{NM}(z_1, n_{p1}, z_3, n_{p2}, z_2) = D_{BM}(z_1, n_{p1}, z_3, n_{p2}) - D_{FM}(z_1, n_{p1}, z_2, n_{p2}). \quad (2)$$

The net mass redistribution function D_{NM} measures the net effect of the halo group size n_{p1} at redshift z_1 on the mass cascade of halo group size n_{p2} from redshift z_2 to z_3 , with $D_{NM} < 0$ indicating that the halo group of size n_{p1} inherits more mass from the halo group size n_{p2} than the mass it passes to the halo group of the same size n_{p2} . Obviously, from Eq. (1),

$$\sum_{n_{p2}} D_{NM}(z_1, n_{p1}, z_2, n_{p2}) = 0. \quad (3)$$

Figure 5 plots the net mass redistribution function D_{NM} for five halo group sizes n_{p1} , with $D_{NM} < 0$ for halo groups n_{p2} smaller than size n_{p1} and $D_{NM} > 0$ for halo groups n_{p2} larger than size n_{p1} . The net effect is that halos are transferring mass from small mass scales to large mass scales, i.e. an inverse mass cascade in the halo mass space. In contrast, the direct mass cascade refers to the transferring of mass from large to small mass scales. In short, three distinct features of inverse mass cascade can be clearly identified:

(i) **Local:** the transferring of mass is local in mass space. Halos inherit/pass their mass mostly from/to halos of the same or similar size. The interaction among halos is shown to be local in mass scale. For large halos, mass cascade proceeds via the merging and breaking between halos of very different sizes. For very small halos, mass cascade proceeds more likely through the interaction between halos of comparable sizes. For any finite time interval Δt , the interaction (merging/breaking) between halos can involve multiple halos of different sizes. However, for an infinitesimal time interval $\Delta t \rightarrow 0$, the interaction is most likely between two halos (halos of a similar size and a single merger). This elementary process can be

quantitatively described by a two-body gravitational collapse model in a separate paper (Xu 2021c).

(ii) Asymmetric: mass transfer across halo groups is a two-way process with mass cascading both upward and downward in the halo mass space. However, the net mass transfer is upward, i.e. the structure formation proceeds in a “bottom-up” fashion. The mass redistribution functions of a given halo size n_{p1} are asymmetric about n_{p1} , with more mass inherited from halo groups smaller than n_{p1} (via halo merging) and less mass inherited from halo groups larger than n_{p1} (via halo breaking-up). Larger size halos accrete their mass from a relatively wider size range of halos, while smaller size halos accrete their mass from a narrower size range of halos.

(iii) Inverse: mass cascade through halo groups of different size is two-way and asymmetric. The net effect is that halos are transferring mass from smaller to larger mass scales with halo merging being dominant over the halo breaking, i.e. an inverse mass cascade.

3.2 Time and mass scales in inverse mass cascade

With major features captured in the previous section, let's now try to develop a few elementary ideas about the time and mass scales for inverse mass cascade. The idea is simple. We observe that there exists a broad spectrum of halo sizes. This can be a direct result to maximize system entropy (Xu 2021b,d). The smallest halos are often created by gravitational collapse at the smallest scale and merging with other halos and passing their mass onto larger halos. The larger halos are themselves transitory and pass their mass to even larger halos, and so on. At every instant t , there is a continuous cascade of mass from the smallest to the largest mass scales that we assumed to be a characteristic mass m_h^* , beyond which the cascaded mass will be primarily consumed (dissipated) to grow the mass of halos.

Let the time scale $\tau_h(m_h, a)$ be the average waiting time of a single merging event with a single merger for halo group of mass $m_h < m_h^*$ at scale factor a . The rate at which mass is passed up from this group is $\varepsilon_m \sim -m_h/\tau_h$ (negative sign for inverse mass cascade). When the system is in statistically steady state, this rate of mass transfer must match exactly the rate of mass injecting into the halo sub-system at the smallest scales $m_h \rightarrow 0$ and the rate of mass dissipation at the largest mass scale m_h^* . If this is not the case, there would be a net accumulation of mass at some intermediate scale below m_h^* . We exclude this possibility because we want the statistical structures of halos to be self-similar and scale free for halo groups of mass less than m_h^* once statistically steady state is established. This means a mass propagation range with halo mass $m_h < m_h^*$,

$$-\varepsilon_m \sim m_h/\tau_h = m_h^*/\tau_h^*, \quad (4)$$

where the mass flux (rate of mass transfer) ε_m should be independent of the halo mass m_h in propagation range ($\varepsilon_m < 0$ reflects the inverse mass cascade from small to large mass scales).

With system in the statistically steady state, halo groups with mass below m_h^* ($m_h < m_h^*$) simply propagate the mass to larger scales without any net accumulation of mass in that group. The total mass in the group $m_g = m_h n_h$ should be time-invariant, where n_h is the number of halos in that group that should also be time-invariant. Mass cascade in this range does not contribute to grow the halo group mass m_g . The average waiting time $\bar{\tau}_h$ (halo lifespan) for a

given halo in the group can be calculated,

$$\begin{aligned} \bar{\tau}_h(m_h, a) &= \sum_{k=1}^{\infty} \frac{k\tau_h}{n_h} \left(\frac{n_h-1}{n_h} \right)^{k-1} \\ &= \frac{\tau_h}{n_h} + \frac{n_h-1}{n_h} \frac{(2\tau_h)}{n_h} + \dots = n_h \tau_h, \end{aligned} \quad (5)$$

where k is the number of time intervals τ_h for that halo to merge with a single merger. All halos in the same group are assumed to merge with a single merger with the same probability during the time interval of τ_h . Now we can introduce a second time scale $\tau_g(m_h, a)$

$$\tau_g(m_h, a) = \bar{\tau}_h(m_h, a) = n_h \tau_h = -m_g/\varepsilon_m, \quad (6)$$

which is the average waiting time (lifespan) for a given halo in halo group of mass scale m_h , or equivalently the time required to cascade the entire mass m_g of that halo group. The time scale τ_g should decrease with increasing m_h with larger halos having shorter lifespans.

Let $M_h(a)$ be the total mass in halo sub-system at physical time t or scale factor a . The third time scale $\tau_M(a)$ is introduced as the time required to cascade entire mass in the halo sub-system,

$$\tau_M(a) = -M_h(a)/\varepsilon_m(a) \sim t, \quad (7)$$

which is expected to be on the order of the current physical time t .

We are now ready to determine the characteristic mass scale m_h^* for mass cascade. Let $\tau_g(m_h, a)$ be the average waiting time for a halo of mass m_h to merge with a single merger of mass m_p at physical time t . The fourth time scale $\tau_f(m_h, a)$ that we will introduce is

$$\tau_f(m_h, a) = \tau_g(m_h, a) n_p = \tau_g(m_h, a) m_h/m_p, \quad (8)$$

where n_p is the number of particles in that given halo. The time scale τ_f approximately represents the average time required to form the entire halo of mass m_h via a sequence of merging events (n_p times) with single mergers of mass m_p . Let's assume a typical halo of mass $m_h^L(t)$ that is constantly growing with the waiting time exactly to be τ_g for every single merging event during its entire mass accretion history. The actual waiting time of halos can be random in nature and either less or greater than τ_g . The mass accretion of that typical halo should read

$$\frac{dm_h^L}{dt} = \frac{m_p}{\tau_g^L} = \frac{n_p^L m_p}{n_p^L \tau_g^L} = \frac{m_h^L}{n_p^L \tau_g^L}, \quad (9)$$

where $\tau_g^L(a) = \tau_g(m_h^L, a)$. We further have (from Eq. (9)),

$$\frac{d \ln m_h^L}{d \ln t} = \frac{t}{n_p^L \tau_g^L} = \frac{t}{\tau_f(m_h^L, a)}, \quad (10)$$

where we should expect $\tau_f(m_h^L, a) \sim t$ if the typical mass $m_h^L(t)$ grows with a power-law rate. Here $n_p^L = m_h^L/m_p$ is the number of particles in that typical halo. It turns out that this is the case (Eq. (51) in Section 4.1). We expect that large halos require more time to form and the time scale τ_f increases with the halo size m_h . Obviously, four time scales we introduced satisfy the inequality

$$\tau_M(a) \geq \tau_f(m_h, a) \geq \tau_g(m_h, a) \geq \tau_h(m_h, a). \quad (11)$$

For small halos with mass $m_h < m_h^*$, we expect the time scale $\tau_f(m_h, a) \ll t$ to allow sufficient time to form these halos before current time t . For halos with mass $m_h > m_h^*$, the time required to form that halo $\tau_f(m_h, a) \gg t$ and these halos are very rare to find at current time t . The time required to form halos of a characteristic

mass m_h^* should be exactly on the order of the current physical time t , i.e. $\tau_f(m_h^*, a) \sim t \sim \tau_M(a)$, from which we can derive,

$$-\frac{m_h^*}{\varepsilon_m} n_h^* n_p^* \sim -\frac{M_h(a)}{\varepsilon_m} \sim \frac{1}{H}, \quad (12)$$

and

$$m_h^* \sim \frac{M_h(a)}{n_h^* n_p^*} \sim -\frac{\varepsilon_m(a)}{H n_h^* n_p^*} \quad \text{or} \quad \frac{M_h(a)}{m_g^*} \sim \frac{m_h^*}{m_p} = n_p^*. \quad (13)$$

Here n_p^* , n_h^* , and m_g^* are the number of particles in halos of the characteristic mass m_h^* , number of halos in halo group of mass m_h^* , and the total mass of that group, respectively. For halos larger than the characteristic mass m_h^* , on average there is not enough time to form. This does not exclude the existence of these large halos because of the random nature of waiting time. In N -body simulations, the total number of particles in the system scales as $N \sim M_h/m_p \sim n_h^* n_p^{*2}$ from Eq. (13). A dimensionless number z_h can be defined for each halo group to reflect the competition between the local rate of mass transfer ($1/\tau_f$) and the Hubble constant H ,

$$z_h = \frac{M_h(a)}{m_g n_p} \sim -\frac{\varepsilon_m(a)}{m_g n_p H} \sim \frac{t}{\tau_f} \quad \text{and} \quad z_h^* = \frac{M_h(a)}{m_g^* n_p^*}, \quad (14)$$

where z_h decreases with halo size and z_h^* for halos with characteristic mass m_h^* should be on the order of one. The exact value of z_h^* can be determined with Eq. (53) ($z_h^* \approx 1/\beta_0$).

In short, two distinct ranges can be identified for inverse mass cascade from time/mass scales: 1) mass propagation range with $m_h < m_h^*$, where the system is in a statistically steady state with a scale-independent mass flux ε_m and a time-invariant group mass $m_g = m_h n_h$ (Fig. 6); 2) mass deposition range with $m_h > m_h^*$, where mass cascaded from small scales is actively consumed to grow halos (Fig. 1). Halo group mass m_g is increasing with time in this range.

4 FORMULATING INVERSE MASS CASCADE

Some fundamental ideas and time and mass scales for inverse mass cascade are presented in the previous section. To understand how the inverse mass cascade quantitatively proceeds, this section will develop these ideas into a rigorous mathematical formulation.

4.1 Mass flux and mass transfer functions

To quantify the mass cascade across halo groups, we first introduce the real-space mass flux function that quantifies the net transfer of mass from all halos smaller than the size m_h to all halos greater than m_h . The mass flux function $\Pi_m(m_h, a)$ can be defined as

$$\Pi_m(m_h, a) = -\frac{\partial}{\partial t} \left[M_h(a) \int_{m_h}^{\infty} f_M(m, m_h^*) dm \right]. \quad (15)$$

Here $M_h(a)$ is the total mass in halo sub-system that increases with scale factor a . The halo mass function $f_M(m_h, a)$ is the probability distribution of total mass $M_h(a)$ with respect to halo mass m_h or n_p (the particle number in halo).

Since halo mass m_h and scale factor a are the only two independent variables for the analysis of the time and mass scales in Section 3.2, the mass function can be written as a function of m_h and a , i.e. $f_M(m_h, a) = f_M(m_h, m_h^*(a))$. The characteristic mass scale $m_h^*(a)$ varies with the scale factor a only, a monotonically increasing function reflecting the fact that larger halos emerge at a later time. The mass flux function Π_m across halo groups should be independent

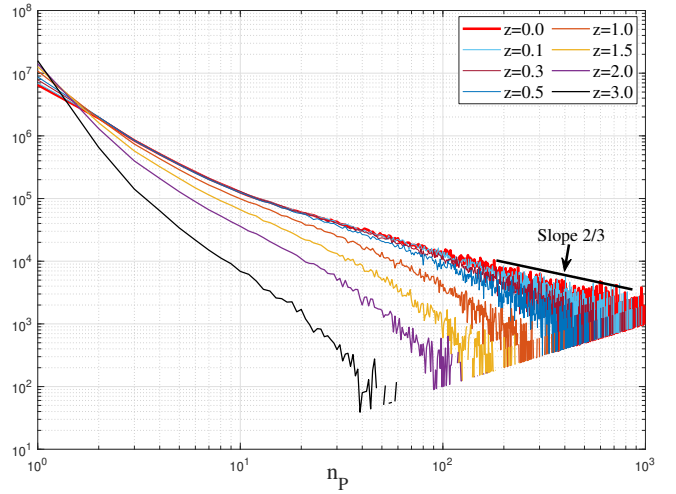


Figure 6. The variation of halo group mass m_g (normalized by particle mass m_p) with group size n_p at different redshift z . At statistically steady state, m_g is not varying with time for halo groups with mass below m_h^* , where mass propagation is dominant. Data for m_g is from halo-based statistical dataset for dark matter flow (Xu 2022a) and is also used to compute rate of mass cascade Π_m in Fig. 10.

of halo size m_h for halo groups smaller than $m_h^*(a)$ (Section 3.2), where the mass flux function reduces to

$$\varepsilon_m(a) = \Pi_m(m_h, a) \quad \text{for} \quad m_h \ll m_h^*. \quad (16)$$

The constant mass flux (or the mass dissipation rate ε_m that is independent of mass scale m_h) cascades mass from the smallest mass scale to the characteristic scale ($0 \ll m_h < m_h^*$) in the mass propagation range. The total mass of halo group of size m_h is

$$m_g(m_h, a) = M_h(a) f_M(m_h, m_h^*) m_p. \quad (17)$$

A direct result of the scale-independent mass flux is that the group mass $m_g(m_h, a)$ of a halo group of size m_h reaches a steady state (Not varying with time, see Eq. (19)). The total mass injected at the smallest mass scale (mass continuously injected from the out-of-halo sub-system into the halo sub-system) is passing through the propagation range and consumed to grow the mass of halo groups above the characteristic mass m_h^* (Fig. 6).

The real-space mass transfer function can be defined as the derivative of mass flux function with respect to halo mass,

$$T_m(m_h, a) = \frac{\partial \Pi_m(m_h, a)}{\partial m_h} = \frac{\partial}{\partial t} \left[M_h(a) f_M(m_h, m_h^*) \right] = \frac{\partial m_g(m_h, a)}{m_p \partial t}, \quad (18)$$

which quantifies the rate of change of group mass $m_g(m_h, a)$. For the mass propagation range,

$$T_m(m_h, a) = 0 \quad \text{and} \quad \frac{\partial m_g(m_h, a)}{\partial t} = 0 \quad \text{for} \quad m_h < m_h^*. \quad (19)$$

The mass transfer function $T_m(m_h, a)$ describes the removal of mass from a small scale and the deposition of mass at a large scale ($T_m(m_h, a) > 0$ for $m_h > m_h^*$).

Since the mass dissipation rate $\varepsilon_m(a)$ is independent of halo size

for $m_h < m_h^*$, we may compute the mass flux function at the smallest scales using Eq. (15) with $m_h = 0$,

$$\varepsilon_m(a) = \Pi_m(m_h = 0, a) = -\frac{\partial M_h(a)}{\partial t} \quad \text{for } m_h < m_h^*. \quad (20)$$

Let the time scale $\tau_h(m_h, a)$ be the average time for a single merging event in a halo group of mass m_h , or equivalently an event frequency $f_h(m_h, a)$. The rate of mass transfer from the scale below m_h to the scale above m_h is,

$$\varepsilon_m(a) = -\alpha_0 m_h f_h(m_h, a) \quad \text{for } m_h \ll m_h^*, \quad (21)$$

where α_0 is a numerical factor on the order of unity. The event frequency $f_h(m_h, a)$ should be proportional to the number of halos in the group (term 1 in Eq. (22)) and the surface area of the halos (term 2). Because the halo interactions in mass space is local, we can assume the mass cascade involves merging events between a halo of similar size and a single merger (Figs. 3 and 4). Halo group with more halos (term 1 in Eq. (22)) and halos with a larger surface area (proportional to m_h^λ , i.e. the term 2 in Eq. (22)) have a greater probability to merge with a single merger,

$$f_h(m_h, a) = \underbrace{f_0(a) M_h(a)}_1 \underbrace{f_M(m_h, m_h^*) \frac{m_p}{m_h} \left(\frac{m_h}{m_p}\right)^\lambda}_2, \quad (22)$$

where $f_0(a)$ is a fundamental frequency for the merging between two single mergers at a given redshift z or scale factor a and may be used to determine dark matter particle mass m_p (Eq. (32)). The characteristic time of a single merging event can be written as $\tau_h(m_h, a) = 1/(\alpha_0 f_h)$.

Without loss of generality, the exponent λ is a halo geometry parameter that represents the effect of halo surface area on the merging frequency $f_h(m_h, a)$. For two halos of very different sizes (merging between a large halo and a single merger), it is estimated that $\lambda = 2/3$ with $m_h \propto r_h^3 \propto A_h^{3/2}$, where A_h is the halo surface area. For small halos, merging is more likely between two halos of comparable sizes where λ can deviate from $2/3$ and approach 1. Halos may be treated as fractal objects with a fractal surface dimension D_h . In principle, $\lambda = D_h/3$ can be related to the fractal dimension D_h that characterizes the degree of roughness of the halo surface. The fractal dimension D_h of the halo surface normally varies between 2 for a perfectly smooth sphere surface to 3 for an extremely porous sphere with surface area proportional to its volume. Small halos tend to be more porous with a greater D_h and geometry parameter λ .

Substitution of Eq. (22) for the event frequency into the Eq. (21) leads to the mass flux,

$$\varepsilon_m(a) = -\alpha_0 f_0(a) M_h(a) f_M(m_h, m_h^*) m_p \left(\frac{m_h}{m_p}\right)^\lambda. \quad (23)$$

For self-similar gravitational clustering in the mass propagation range ($m_h < m_h^*$), the halo mass m_h and characteristic mass scale m_h^* are the only two controlling variables and we can simply express the mass function as $f_M(m_h, m_h^*) \sim (m_h)^x (m_h^*)^{-x-1}$. Now using dimensional analysis, the only possible form of the mass function f_M that satisfies Eq. (23) is (f_M should have a unit of $1/\text{kg}$ in SI units and ε_m is a function of a only and is independent of m_h),

$$f_M(m_h, m_h^*) = \beta_0 m_h^{-\lambda} (m_h^*)^{\lambda-1} \quad \text{for } m_h < m_h^*, \quad (24)$$

where $\beta_0 \sim O(1)$ is a numerical constant. The mass flux and event frequency in the mass propagation range can be expressed as (after

substituting Eq. (24) into (23)),

$$\varepsilon_m(a) = -\alpha_0 \beta_0 \lambda_0 N m_p f_0(a) \quad \text{for } m_h < m_h^*, \quad (25)$$

and

$$f_h(m_h, a) = \beta_0 \lambda_0 f_0(a) N m_p / m_h \quad \text{for } m_h < m_h^*, \quad (26)$$

where a dimensionless constant λ_0 is defined as

$$\lambda_0 = \frac{M_h(a)}{N m_p} \left(\frac{m_h^*}{m_p}\right)^{\lambda-1}, \quad (27)$$

which is a time-invariant constant and dependent only on the mass resolution m_p . For $m_p = 2.27 \times 10^{11} M_\odot / h$ from Table 1 and $m_h^*(z=0) \approx 2 \times 10^{13} M_\odot / h$, λ_0 is on the order of 0.13. The halo group mass in the propagation range (from Eq. (24)) should be

$$m_g(m_h, a) \equiv m_g(m_h) = \lambda_0 \beta_0 N m_p (m_p / m_h)^\lambda. \quad (28)$$

Equivalently, we have

$$m_g(m_p) = \lambda_0 \beta_0 N m_p, \quad m_g(m_h) = m_g(m_p) (m_p / m_h)^\lambda \quad (29)$$

for the group mass of single mergers with $m_h = m_p$. The group mass m_g is proportional to $m_h^{-\lambda}$ (Fig. 6). The relation between the rate of change of mass M_h and m_h^* can be found from Eq. (27),

$$\frac{\partial \ln M_h}{\partial \ln a} = (1 - \lambda) \frac{\partial \ln m_h^*}{\partial \ln a}. \quad (30)$$

With Eqs. (20) and (27), we may derive the mass dissipation rate as a function of m_h^* ,

$$\begin{aligned} \varepsilon_m(a) &= -(1 - \lambda) \frac{\partial \ln m_h^*}{\partial \ln a} H(a) M_h(a) \\ &= -\lambda_0 (1 - \lambda) \frac{\partial \ln m_h^*}{\partial \ln a} H(a) N m_p \left(\frac{m_h^*}{m_p}\right)^{1-\lambda}. \end{aligned} \quad (31)$$

With Eqs. (25) and (31), we find the fundamental frequency $f_0(a)$ as a function of m_h^* ,

$$f_0(a) = \frac{(1 - \lambda)}{\alpha_0 \beta_0} \frac{\partial \ln m_h^*}{\partial \ln a} H(a) \left(\frac{m_h^*}{m_p}\right)^{1-\lambda}, \quad (32)$$

that is also related to the Hubble constant $H(a)$ and mass resolution m_p . The characteristic time scale $\tau_h^* = \tau_h(m_h^*, a)$ associated with the characteristic mass m_h^* is

$$\tau_h^*(a) = -\frac{m_h^*}{\varepsilon_m} = \frac{1/(\lambda_0 (1 - \lambda))}{N \frac{\partial \ln m_h^*}{\partial \ln a} H} \left(\frac{m_h^*}{m_p}\right)^\lambda. \quad (33)$$

The fundamental frequency $f_0(a)$ is the frequency for the elementary merging between two single mergers and is expected to decrease with time. Without loss of generality, let's assume a power-law of $f_0(a) \propto a^{-\tau_0}$ that leads to $\varepsilon_m(a) \propto a^{-\tau_0}$ (Eq. (25)), $\left(\frac{m_h^*}{m_p}\right)^{1-\lambda} \propto a^{3/2-\tau_0}$ (Eq. (31)), and $M_h(a) \propto a^{3/2-\tau_0}$ (Eq. (27)). Once the statistically steady state is established for inverse mass cascade, the total mass of halo sub-system increases as $M_h(a) \propto a^{3/2-\tau_0}$ regardless of the value of λ . Obviously,

$$\frac{\partial \ln M_h}{\partial \ln a} = (1 - \lambda) \frac{\partial \ln m_h^*}{\partial \ln a} = \frac{3}{2} - \tau_0 > 0. \quad (34)$$

With total mass in halo sub-system $M_h(a)$ increasing with the scale factor a , it requires $0 < \tau_0 < 3/2$. With $\tau_0 > 0$ and $a \rightarrow \infty$, the mass flux $\varepsilon_m(a)$ approaches to zero with the entire system approaches the limiting thermodynamic equilibrium but can never reach. In this

regard, the everlasting inverse mass cascade is a key feature of the statistically (intermediate) steady state when system evolves toward the limiting equilibrium.

Number of halos $n_h(m_h)$ in halo group with a given mass m_h is

$$n_h(m_h) \equiv m_g(m_h)/m_h = \lambda_0 \beta_0 N m_h^{-\lambda-1} m_p^{\lambda+1}, \quad (35)$$

which does not vary with time once the statistically steady state is established. Substitution of Eq. (34) into Eq. (32), we can express the fundamental frequency $f_0(a)$ as,

$$f_0(a) = \frac{1}{\alpha_0 \beta_0} \left(\frac{3}{2} - \tau_0 \right) H(a) \left(\frac{m_h^*}{m_p} \right)^{1-\lambda} = \frac{b_0}{\alpha_0 \beta_0} H_0 a^{-\tau_0}, \quad (36)$$

where the mass resolution parameter b_0 can be related to a fixed characteristic mass $m_h^*(a)$ at $a=1$,

$$b_0 = \left(\frac{3}{2} - \tau_0 \right) \left(\frac{m_h^*(a=1)}{m_p} \right)^{1-\lambda}, \quad (37)$$

which is dependent on the mass resolution m_p only (the mass of dark matter particle), with smaller particle mass m_p giving rise to a greater fundamental frequency $f_0(a)$ in N -body simulation. For mass resolution of $m_p = 2.27 \times 10^{11} M_\odot/h$ from Table 1 and $m_h^*(a=1) = 2 \times 10^{13} M_\odot/h$, $b_0 \approx 2.2$ with $\tau_0 = 1$. In other words, the dark matter particle mass can be determined if the fundamental frequency $f_0(a)$ can be precisely measured.

Now we can introduce a numerical constant,

$$c_0 = b_0 \lambda_0 = \left(\frac{3}{2} - \tau_0 \right) \frac{M_h(a)}{N m_p} a^{\tau_0-3/2}, \quad (38)$$

which is the mass fraction of halo sub-system $M_h(a)$ and not dependent on the mass resolution m_p and scale factor a . We estimate $c_0 \approx 0.29$ with $\tau_0 = 1$, i.e. $M_h \approx 0.58 N m_p$ when $a=1$. This information is used to study the density distributions for particles in halos and out-of-halos, respectively (Xu 2022i).

Finally we present the simplified expressions for time and mass scales and mass flux function that can be fully described as functions of halo mass m_h , scale factor a , and mass resolution m_p with four numerical constants β_0 (pre-factor for halo mass function f_M), c_0 (the mass fraction of halo sub-system), λ (the halo geometry parameter), and τ_0 (the exponent of the fundamental frequency f_0), and the characteristic mass $m_h^*(a=1)$ and H_0 ,

$$\varepsilon_m(a) = - \left(\frac{3}{2} - \tau_0 \right) H(a) M_h(a) = -c_0 H_0 N m_p a^{-\tau_0}, \quad (39)$$

$$\tau_h^*(a) = \frac{1/(N \lambda_0 H(a))}{(3/2 - \tau_0)} \left(\frac{m_h^*}{m_p} \right)^\lambda = \frac{m_h^*(a=1)}{c_0 H_0 N m_p} a^{\frac{(3/2-\tau_0)}{(1-\lambda)}}, \quad (40)$$

$$m_h^*(a) = \left(\frac{b_0}{3/2 - \tau_0} \right)^{\frac{1}{1-\lambda}} a^{\frac{(3/2-\tau_0)}{(1-\lambda)}} m_p = m_h^*(a=1) a^{\frac{(3/2-\tau_0)}{(1-\lambda)}}, \quad (41)$$

$$M_h(a) = \frac{c_0}{3/2 - \tau_0} N m_p a^{(3/2-\tau_0)}. \quad (42)$$

Let us revisit the time scales we introduced in Section 3.2. The time scale $\tau_M(a)$ is

$$\tau_M(a) = - \frac{M_h(a)}{\varepsilon_m(a)} = \frac{3/2}{3/2 - \tau_0} a^{3/2} t_0 = \frac{3/2}{3/2 - \tau_0} t, \quad (43)$$

which is the time it takes to cascade all mass in the halo sub-system at a given scale factor a and $\tau_M(a)$ is on the order of t . This relation might be used to determine the value of τ_0 from N -body simulations.

Time scale τ_h for a single merging in halo group of mass m_h is,

$$\tau_h(m_h, a) = \frac{m_h}{\varepsilon_m} = \frac{m_h/(\alpha_0 \beta_0 \lambda_0)}{f_0(a) N m_p} = \frac{m_h}{c_0 H_0 N m_p} a^{\tau_0}. \quad (44)$$

The time scale τ_g that takes to cascade the group mass m_g for the halo group of mass m_h is,

$$\begin{aligned} \tau_g(m_h, a) &= \frac{m_h n_h}{\varepsilon_m} = \frac{1}{\alpha_0 f_0(a)} \left(\frac{m_h}{m_p} \right)^{-\lambda} \\ &= \frac{\beta_0}{(3/2 - \tau_0) H_0} \frac{m_h^{-\lambda} m_p}{[m_h^*(a=1)]^{1-\lambda}} a^{\tau_0}. \end{aligned} \quad (45)$$

As expected, the mean waiting time (lifespan) τ_g of a given halo is decreasing with halo mass as $\tau_g \propto m_h^{-\lambda}$ and increasing with a . Larger halos have a shorter lifespan. Extremely large halos have very fast mass accretion and infinitesimal lifespan that lead to isothermal density (Xu 2021a).

The time scale τ_f is introduced as the average time it takes to form the halo of mass m_h that reads

$$\begin{aligned} \tau_f(m_h, a) &= \frac{m_h n_h n_p}{\varepsilon_m} = \frac{1}{\alpha_0 f_0(a)} \left(\frac{m_h}{m_p} \right)^{1-\lambda} \\ &= \frac{\beta_0}{(3/2 - \tau_0) H_0} \left(\frac{m_h}{m_h^*(a=1)} \right)^{1-\lambda} a^{\tau_0}, \end{aligned} \quad (46)$$

which increases with halo mass as $m_h^{1-\lambda}$. The relation between time scales $\tau_f(m_h^*, a) = \beta_0 \tau_M(a)$ can be easily obtained from Eqs. (43) and (46) that is consistent with our analysis in Section 3.2 (Eq. (13)), i.e. $\beta_0 M_h(a) = m_g^* n_p^* = n_h^* n_p^{*2} m_p$ and $z_h^* \beta_0 = 1$ (from Eq. (14)). Different time scales can be related to the mass flux function as,

$$\varepsilon_m = \frac{-M_h(a)}{\tau_M(a)} = \frac{-m_g(m_h)}{\tau_g(m_h, a)} = \frac{-m_g n_p}{\tau_f(m_h, a)} = \frac{-m_h}{\tau_h(m_h, a)}. \quad (47)$$

The corresponding time scales at characteristic mass m_h^* are

$$\tau_g^*(a) = \frac{\beta_0 m_p}{(3/2 - \tau_0) H_0 m_h^*(a=1)} a^{\frac{\tau_0-3\lambda/2}{1-\lambda}}, \quad (48)$$

$$\tau_f^*(a) = \frac{\beta_0}{(3/2 - \tau_0) H}. \quad (49)$$

The two time scales $\tau_g \propto a^{\tau_0} m_h^{-\lambda}$ (Eq. (45)) and $\tau_f \propto a^{\tau_0} m_h^{1-\lambda}$ (Eq. (46)), where larger halos have shorter lifespan but take more time to form. For $\lambda = 2/3$ and $\tau_0 = 1$, the lifespan τ_g^* of characteristic halos is independent of time.

Now we can track the growth of typical halos by integrating Eq. (9) with respect to the scale factor a and using expression of time scale τ_g (Eq. (45)) with initial condition $m_h^L(a=0) = 0$ to obtain

$$\frac{m_h^L(a)}{m_h^*(a=1)} = \left(\frac{1-\lambda}{\beta_0} \right)^{1/(1-\lambda)} a^{\frac{3/2-\tau_0}{1-\lambda}} \quad (50)$$

and

$$\frac{m_h^L(a)}{m_h^*(a)} = \left(\frac{1-\lambda}{\beta_0} \right)^{1/(1-\lambda)},$$

which follows the same scaling as characteristic mass scale $m_h^*(a)$. For large halos with $\tau_0 = 1$ and $\lambda = 2/3$, $m_h^L(a) \sim m_h^*(a) \sim a^{3/2}$. This scaling matches the mass growth of type II halos, i.e the dominant type for large halos (see McBride et al. 2009, Fig. 2), as shown in Fig. 7.

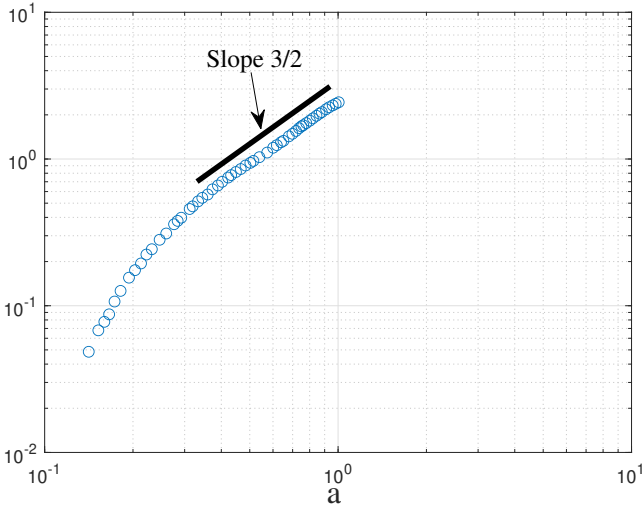


Figure 7. The halo mass (normalized by $10^{12} M_{\odot}$) accretion history for type II halos, i.e. the dominant type for large halos (see McBride et al. 2009, Fig. 2), exhibits a power law scaling $\propto a^{3/2}$ once the statistically steady state is established in dark matter flow.

With the help of Eq. (10), we confirm that time scale τ_f (Eq. (46)) to form the typical halo is on the same order of t (Eq. (10)),

$$\tau_f(m_h^L, a) = \frac{1 - \lambda}{1 - 2\tau_0/3} t \sim t. \quad (51)$$

Finally, it can be easily confirmed that (from Eq. (31)),

$$\varepsilon_m(a) = -\frac{dM_h(a)}{dt} = -\left(\frac{3}{2} - \tau_0\right) H M_h(a). \quad (52)$$

The relations between total mass of all halos M_h , typical halo mass m_h^L , and mass scale m_h^* are (from Eqs. (27), (35) and (50)),

$$M_h(a) = \frac{1}{1 - \lambda} m_h^L n_h^L n_p^L = \frac{1}{\beta_0} m_h^* n_h^* n_p^*, \quad (53)$$

where total halo mass M_h is related to the mass of typical halo m_h^L or characteristic mass m_h^* . The mass flux function $\varepsilon_m(a)$ can be simply interpreted as the rate of mass change of a typical halo m_h^L or m_h^* multiplied by the equivalent number of that halo in the system,

$$\begin{aligned} \varepsilon_m(a) &= -\frac{dm_h^L}{dt} n_h^L n_p^L = -\frac{d(m_h^L n_h^L n_p^L)}{(1 - \lambda) dt} \\ &= -\lambda_0 \beta_0 N \frac{dm_h^L}{dt} \left(\frac{m_h^L}{m_p}\right)^{-\lambda} \end{aligned} \quad (54)$$

or

$$\begin{aligned} \varepsilon_m(a) &= -\frac{1 - \lambda}{\beta_0} \frac{dm_h^*}{dt} n_h^* n_p^* = -\frac{d(m_h^* n_h^* n_p^*)}{\beta_0 dt} \\ &= -\lambda_0 (1 - \lambda) N \frac{dm_h^*}{dt} \left(\frac{m_h^*}{m_p}\right)^{-\lambda}. \end{aligned} \quad (55)$$

In summary, the mathematical model for inverse mass cascade provides the complete dependence of time/mass scales and mass flux/transfer functions on the scale factor a , halo mass m_h , and mass resolution m_p . An interesting case is that $\tau_0 = 1$, where the fundamental frequency $f_0(a) \propto a^{-1}$. Note that this is the same scaling as the photon frequency decaying due to the cosmological redshift.

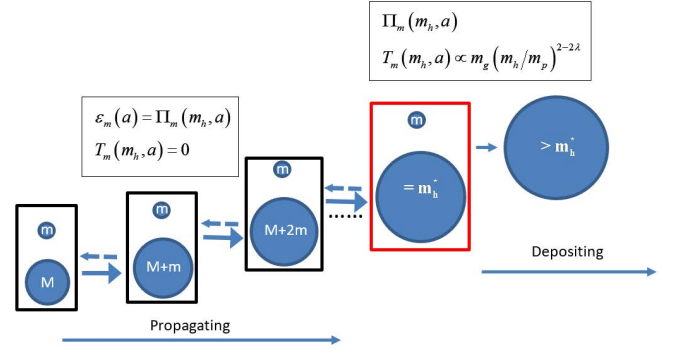


Figure 8. Schematic plot of a chain reaction description for inverse mass cascade. Halos merge with free radicals (single mergers) to cause the next merging along the chain and facilitate a continuous mass cascade. Mass flux function $\Pi_m(m_h, a)$ can be computed using halo mass function at different z . A constant mass flux $\varepsilon_m(a)$ is expected for halos smaller than characteristic mass ($m_h < m_h^*$) in mass propagation range. Mass cascaded from small scales is consumed to grow halo mass at scales $m_h > m_h^*$.

Table 2 lists the scaling exponents with respect to a for different values of τ_0 and λ . The scaling of $\varepsilon_m(a)$, $f_0(a)$ and $M_h(a)$ are only dependent on τ_0 , while $m_h^*(a)$ and $\tau_h^*(a)$ depend on both τ_0 and λ . Table 3 summarizes the dependence on the halo size m_h , where $\tau_g \sim m_h^{-\lambda}$ and $\tau_f \sim m_h^{1-\lambda}$. Table 4 presents the dependence of relevant parameters on the mass resolution m_p .

4.2 Chain reaction and random walk for inverse mass cascade

The chain reaction model is often used to describe a sequence of reactions where the reactive product will cause the next reaction in the sequence. Chain reactions provide non-equilibrium systems a potential mechanism to continuously release energy and increase system entropy. The model can be mathematically represented by Markov chains and generally involves three stages: initiation, propagation, and termination. Particularly for SG-CFD, we can describe the inverse mass cascade as follows (See Fig. 8),

(i) The initial stage corresponds to the initiation/generation of the chain carriers (free radicals) to provide mass and energy source for the halo sub-system; Most N -body simulations start with a fixed number of chain carriers (free radicals) generated initially. However, continuous generation of free radicals at the smallest scale should be required to sustain a continuously everlasting inverse mass cascade process ($M_h(a) \propto a^{(3/2-\tau_0)}$ in Eq. (42)) once the statistically steady state is established. It mimics the forced homogeneous isotropic turbulence, where a continuous injection of energy at the integral scale balances the energy dissipated at the smallest scale. The potential mechanisms to generate such free radicals at the smallest scale can be a direct cascade process from large to small scales or a direct generation of radicals at the smallest scale (i.e. Planck scale). Despite the unknown mechanism, the rate of generation at the smallest scale should be $-\varepsilon_m$ that matches the mass flux across halos.

(ii) The propagation stage ($m_h < m_h^*$) involves a sequence of merging with single mergers to propagate mass along the reaction chain (mass propagation range), where the dominant mode is mass propagation. The group mass m_g is time-invariant in this stage. For a given halo group of mass m_h , group mass m_g equals a critical group mass

λ	τ_0	f_0	ε_m	M_h	f_M	m_h^*	τ_h^*	n_h^*	m_g^*	τ_g^*
λ	τ_0	$a^{-\tau_0}$	$a^{-\tau_0}$	$a^{3/2-\tau_0}$	$a^{\tau_0-3/2}$	$a^{\frac{(3/2-\tau_0)}{(1-\lambda)}}$	$a^{\frac{(3/2-\lambda\tau_0)}{(1-\lambda)}}$	$a^{-\left(\frac{3}{2}-\tau_0\right)\frac{(1+\lambda)}{(1-\lambda)}}$	$a^{-\left(\frac{3}{2}-\tau_0\right)\frac{\lambda}{(1-\lambda)}}$	$a^{\frac{(\tau_0-3\lambda/2)}{(1-\lambda)}}$
2/3	1	a^{-1}	a^{-1}	$a^{1/2}$	$a^{-1/2}$	$a^{3/2}$	$a^{3/2}$	$a^{-5/2}$	a^{-1}	a^0
2/3	1/2	$a^{-1/2}$	$a^{-1/2}$	a^1	a^{-1}	a^3	$a^{7/2}$	a^{-5}	a^{-2}	$a^{-3/2}$
3/4	1	a^{-1}	a^{-1}	$a^{1/2}$	$a^{-1/2}$	a^2	a^3	$a^{-7/2}$	$a^{-3/2}$	$a^{-1/2}$

Table 2. Dependence on the scale factor a for different values of τ_0 and λ

f_M	ε_m	f_h	τ_h	τ_g	τ_f	m_g	n_h
$m_h^{-\lambda}$	m_h^0	m_h^{-1}	m_h^1	$m_h^{-\lambda}$	$m_h^{1-\lambda}$	$m_h^{-\lambda}$	$m_h^{-1-\lambda}$

Table 3. Dependence on the halo mass m_h

f_M	f_h	τ_f	ε_m	τ_h^*	τ_h	m_h^*	M_h	c_0	β_0
m_p^0	m_p^0	m_p^0	m_p^0	m_p^0	m_p^0	m_p^0	m_p^0	m_p^0	m_p^0
n_h	τ_g	m_g	n_p	f_0	b_0	λ_0	n_h^*	m_g^*	n_p^*
m_p	m_p	m_p	m_p^{-1}	$m_p^{\lambda-1}$	$m_p^{\lambda-1}$	$m_p^{1-\lambda}$	m_p	m_p	m_p^{-1}

Table 4. Dependence on the mass resolution m_p

m_g^c (Eqs. (27), (28), and (24))

$$m_g(m_h) = \beta_0 \lambda_0 N m_p (m_h/m_p)^{-\lambda} \quad (56)$$

$$= m_g^c(m_h) = M_h(a) f(m_h, m_h^*) m_p$$

that is required to sustain the forward propagation along the chain. The mass propagation range is fully described in Section 4.1.

(iii) The termination stage ($m_h > m_h^*$) involves the consumption (deposition) of mass cascaded from the scales below m_h^* to scales larger than m_h^* (deposition range). At this stage, since there is not enough time to form halo larger than m_h^* , the group mass for halo groups of $m_h > m_h^*$ is lower than the critical group mass ($m_g < m_g^c$) required to sustain the propagation (sub-critical mass in the terminology of chain reaction). The dominant mode in this stage is the growth of halo group mass (mass deposition range).

Based on the chain reaction description, the idea of inverse mass cascade can be further refined in terms of a random walk of halos in mass space to include both propagation and deposition range. Halos are migrating in mass space due to the merging with single mergers with a given distribution of waiting time (or the jumping frequency). Now let us consider that distribution in more details.

The mean time interval of a single merging for halo group of mass m_h is $\tau_h \sim m_h^{-\lambda}/n_h$ from Eq. (45). Let the actual time interval of a single merging for a given halo be a random variable τ_{gr} with its mean given by $\tau_g = \langle \tau_{gr} \rangle = n_h \tau_h \gg \tau_h$ (from Eq. (5)). Typical halos discussed before have a direct delta distribution with a deterministic $\tau_{gr} \equiv \tau_g$. The probability distribution of time $\tau_{gr} = k \tau_h$ can be described by a discrete distribution $P(k, n_h)$, where k is the number of time interval τ_h for a given halo to wait till the first merging with a single merger (See Eq. (5)),

$$P(k, n_h) = P_r(X = k) = \frac{1}{n_h} \left(1 - \frac{1}{n_h}\right)^{k-1} \quad (57)$$

with $\sum_{k=1}^{\infty} P(k, n_h) = 1$.

The cumulative function and moments of the probability mass func-

tion $P(k, n_h)$ are given by,

$$Q(k, n_h) = \sum_{m=1}^k P(m, n_h) = 1 - \left(1 - \frac{1}{n_h}\right)^k \quad (58)$$

$$\langle k \rangle = \sum_{k=1}^{\infty} [P(k, n_h) k] = n_h, \quad (59)$$

$$\langle k^2 \rangle = \sum_{k=1}^{\infty} [P(k, n_h) k^2] = n_h (2n_h - 1), \quad (60)$$

$$\langle k^m \rangle = \sum_{k=1}^{\infty} [P(k, n_h) k^m] = \frac{\text{PolyLog}(-m, 1 - 1/n_h)}{n_h - 1}. \quad (61)$$

The probability distribution of time interval τ_{gr} of a given halo finally reads (from Eq. (57)),

$$P(\tau_{gr}, n_h) = \frac{1}{n_h} \left(1 - \frac{1}{n_h}\right)^{\frac{n_h \tau_{gr}}{\tau_g} - 1} \approx \frac{1}{n_h} \exp\left(-\frac{\tau_{gr}}{\tau_g}\right), \quad (62)$$

with the mean $\tau_g \sim m_h^{-\lambda}$. The exponential distribution of waiting time τ_{gr} is obtained by taking the limit $n_h \rightarrow \infty$. The probability density function of the continuous random waiting time τ_{gr} reads

$$P(\tau_{gr}) = \frac{1}{\tau_g} \exp\left(-\frac{\tau_{gr}}{\tau_g}\right). \quad (63)$$

Clearly, exponential distribution of waiting time τ_{gr} for a given halo is dependent on τ_g (Eq. (45)). Therefore, the distribution of τ_{gr} is dependent on mass m_h of that halo (i.e. random walk with a position-dependent waiting time), scale factor a , geometry exponent λ , and parameter τ_0 .

For this simple description of inverse mass cascade, the distribution of the random waiting time τ_{gr} (Eq. (63)) is dependent on the position of random walker in mass space (i.e. mass m_h). Therefore, a heterogeneous diffusion model can be naturally used to describe the mass cascade with a position-dependent diffusivity. The formulation starts from the (no inertia) Markovian overdamped Langevin equation describing the random walk in halo mass space,

$$\frac{\partial m_h(t)}{\partial t} = \frac{m_p \xi_n(t)}{\tau_{gr}}, \quad (64)$$

where $\tau_{gr}(t)$ is the random waiting time with an exponential distribution in Eq. (63) and $\xi_n(t)$ is a dimensionless standard normal variable. The random variable $1/\tau_{gr}$ has a probability density of

$$P\left(x = \frac{1}{\tau_{gr}}\right) = \frac{1}{x^2 \tau_g} \exp\left(-\frac{1}{x \tau_g}\right). \quad (65)$$

We can roughly approximate the random variable $1/\tau_{gr}$ with a Gaussian variable ξ'_n

$$\frac{1}{\tau_{gr}} \approx \frac{1}{a_g \tau_g} \left(1 + \xi'_n\right) \quad (66)$$

such that the original Eq. (64) becomes

$$\frac{\partial m_h(t)}{\partial t} = \frac{m_p \xi_n(t)}{\tau_{gr}} \approx \frac{m_p \xi(t)}{\tau_g} \left(1 + \xi'_n(t)\right), \quad (67)$$

where the constant $a_g \approx 2$ is absorbed into a new Gaussian variable $\xi(t) = \xi_n(t)/a_g$. The random noise term $\xi'_n(t)$ in Eq. (67) comes from the fact that the waiting time $\tau_{gr}(t)$ is an exponential random variable. By neglecting the term $\xi'_n(t)$ and for a power-law position-dependence ($\tau_g \propto m_h^{-\lambda}$), the first order approximation of the evolution of halo mass m_h reads

$$\frac{\partial m_h(t)}{\partial t} = \frac{m_p \xi(t)}{\tau_g(m_h)} = \sqrt{2D_p(m_h)} \zeta(t), \quad (68)$$

where the position-dependent diffusivity

$$D_p(m_h) = D_{p0} m_h^{2\lambda} = \alpha_p m_p^2 t (\tau_g)^{-2}. \quad (69)$$

Here D_{p0} is a proportional constant for the diffusivity D_p and α_p is a dimensionless constant with its expression provided in Eq. (84). The random noise $\xi(t)$ is dimensionless and

$$\xi(t) = \sqrt{2\alpha_p t} \zeta(t), \quad (70)$$

where the white Gaussian noise $\zeta(t)$ satisfies the covariance $\langle \zeta(t) \zeta(t') \rangle = \delta(t - t')$ with a zero mean $\langle \zeta(t) \rangle = 0$. Equation (68) describes the stochastic evolution of halo mass m_h with a deterministic waiting time $\tau_g(m_h)$ for every step of random walk. However, there exist halos deviated from this evolution path due to the random nature of τ_{gr} or the perturbation term $\xi'_n(t)$ in Eq. (67) that is currently neglected. This will give rise to the stochastic halo size evolution that will be discussed in a separate paper (Xu 2021a). While we only focus on the solution of stochastic Eq. (68) in this paper, a continuous-time random walks (CTRW) may be explored to gain more insights into the original Eq. (64) in the future.

In Stratonovich interpretation (Stratonovich 1966), the Langevin equation (Eq. (68)) yields to a probability distribution $P_h(m_h, t)$ satisfying the differential equation (Fokker-Planck equation)

$$\begin{aligned} \frac{\partial P_h}{\partial t} &= \frac{\partial}{\partial m_h} \left[\sqrt{D_p} \frac{\partial}{\partial m_h} \left(\sqrt{D_p} P_h \right) \right] \\ &= D_{p0} \frac{\partial}{\partial m_h} \left[m_h^\lambda \frac{\partial}{\partial m_h} \left(m_h^\lambda P_h \right) \right], \end{aligned} \quad (71)$$

which describes the probability of halo with a given mass m_h from random walk in mass space. Next section will discuss the heterogeneous diffusion model for halo mass function.

4.3 Heterogeneous diffusion model and halo mass functions

The heterogeneous diffusion with spatially dependent diffusivity plays an important role for many physical problems. Examples are the mass transport in porous, inhomogeneous media and in plasmas. The transport in these examples involves the waiting time that is explicitly dependent on the position. Particularly, the power-law dependence of the diffusivity is natural for many systems exhibiting self-similarity, for example the disordered materials, the diffusion on fractals, and the mass cascade of self-gravitating collisionless dark matter flow (SG-CFD) in this work. Here a heterogeneous diffusion model can be established for inverse mass cascade with waiting time explicitly dependent on the halo mass ($\tau_g \sim m_h^{-\lambda}$). First, the group mass m_g for halo groups reads

$$m_g(m_h, a) = M_h(a) f_M(m_h, a) m_p, \quad (72)$$

where M_h is the total mass in halo sub-system, $f_M(m_h, a)$ is the probability distribution with respect to the halo mass m_h (mass function), and m_p is the mass resolution (particle mass). The time variation of m_g has two contributions from Eq. (72),

$$\frac{\partial m_g}{\partial a} = \underbrace{M_h(a) m_p \frac{\partial f_M}{\partial a}}_1 + \underbrace{f_M(m_h, a) m_p \frac{\partial M_h}{\partial a}}_2, \quad (73)$$

where term 1 is due to the time variation of $f_M(m_h, a)$ and term 2 from the variation of total mass M_h . For position-dependent power-law diffusivity $D_{md} = D_{m0} m_h^{2\lambda}$, the dynamics of m_g can be described by the heterogeneous diffusion model (From Eq. (71) with $f_M = P_h$ and transforming the derivative from t to a),

$$\frac{\partial m_g}{\partial a} = \underbrace{\frac{\partial}{\partial m_h} \left[\sqrt{D_{m0}} m_h^\lambda \frac{\partial}{\partial m_h} \left(\sqrt{D_{m0}} m_h^\lambda m_g \right) \right]}_1 + \underbrace{\frac{\partial \ln M_h}{\partial \ln a} \frac{m_g}{a}}_2, \quad (74)$$

where term 1 describes the heterogeneous diffusion of m_g in mass space and term 2 describes the source term due to the increasing total mass M_h in all halos. The boundary conditions are:

$$\frac{\partial m_g}{\partial a} \Big|_{m_h=0} = \frac{m_p}{H a} T_m|_{m_h=0} = 0, \quad (75)$$

$$-\frac{1}{m_p} \frac{\partial}{\partial a} \int_0^\infty m_g(m_h, a) dm_h \equiv \frac{\varepsilon_m}{H a} = -\frac{\partial M_h}{\partial a}. \quad (76)$$

The governing equation for the mass function $f_M(m_h, a)$ can be eventually found with substitution of Eq. (72) into Eq. (74),

$$\frac{\partial f_M(m_h, a)}{\partial a} = D_{m0} \frac{\partial}{\partial m_h} \left[m_h^\lambda \frac{\partial}{\partial m_h} \left(m_h^\lambda f_M \right) \right]. \quad (77)$$

The solution to Eq. (77) is a stretched Gaussian function that has an exponential cut-off for large halo mass m_h and a power-law behavior for small m_h ,

$$f_M(m_h, a) = \frac{m_h^{-\lambda}}{\sqrt{\pi D_{m0} a}} \exp \left[-\frac{m_h^{2-2\lambda}}{(2-2\lambda)^2 D_{m0} a} \right]. \quad (78)$$

The mean square displacement of m_h in mass space can be defined

$$\begin{aligned} \langle m_h^2 \rangle &= \int_0^\infty f_M(m_h, a) m_h^2 dm_h \\ &= \frac{1}{\sqrt{\pi}} \Gamma \left(\frac{3-\lambda}{2-2\lambda} \right) (2-2\lambda)^{\frac{2}{1-\lambda}} (D_{m0} a)^{\frac{1}{1-\lambda}} \equiv \gamma_0 m_h^{*2}, \end{aligned} \quad (79)$$

where m_h^* is the characteristic mass scale and γ_0 is a proportional constant. With the exponent of $1/(1-\lambda) \geq 1$ in Eq. (79), diffusion in mass space is of a super-diffusion nature. Solution of $f_M(m_h, a)$ (Eq. (78)) can be further expressed in terms of m_h^* ,

$$f_M(m_h, a) = \frac{(1-\lambda)}{\sqrt{\pi \eta_0}} \left(\frac{m_h^*}{m_h} \right)^\lambda \frac{1}{m_h^*} \exp \left[-\frac{1}{4\eta_0} \left(\frac{m_h}{m_h^*} \right)^{2-2\lambda} \right], \quad (80)$$

where the dimensionless constant η_0

$$\eta_0 = \frac{1}{4} \left[\frac{\gamma_0 \sqrt{\pi}}{\Gamma((3-\lambda)/(2-2\lambda))} \right]^{1-\lambda}. \quad (81)$$

For $\lambda = 2/3$ and $\gamma_0 = 15$, we have $\eta_0 = 0.5$. We also found the constant β_0 in the mass propagation range (in Eq. (24)) as,

$$\beta_0 = (1-\lambda)/\sqrt{\pi \eta_0} \approx 0.266. \quad (82)$$

Since m_h^* is related to the mean square displacement of halo mass, diffusivity in halo mass space can be expressed in terms of m_h^* ,

$$D_{m0} = \frac{\eta_0 m_h^{*(2-2\lambda)}}{(1-\lambda)^2 a} \sim a^{2-2\tau_0}. \quad (83)$$

For a constant diffusivity D_{m0} with respect to a , we also would expect $\tau_0 = 1$, i.e. the fundamental frequency $f_0(a) \sim a^{-1}$. The dimensionless constant α_p in Eq. (69) can be found by comparing Eqs. (77) with (71) and using Eqs. (45), (41), and (82),

$$\alpha_p = \frac{3\eta_0 \beta_0^2}{2(1-\lambda)^2(3/2-\tau_0)^2} = \frac{3}{2\pi(3/2-\tau_0)^2}. \quad (84)$$

The k th moments of the mass function f_M can be easily obtained as,

$$\begin{aligned} \int_0^\infty f_M(m_h, a) (m_h)^k dm_h \\ = \frac{1}{\sqrt{\pi}} (4\eta_0)^{\frac{k}{(2-2\lambda)}} \Gamma\left(\frac{k-\lambda+1}{2-2\lambda}\right) (m_h^*)^k, \end{aligned} \quad (85)$$

where in particular, the mean halo mass is proportional to the characteristic mass scale m_h^* ,

$$\langle m_h \rangle = \frac{1}{\sqrt{\pi}} (4\eta_0)^{\frac{1}{(2-2\lambda)}} \Gamma\left(\frac{2-\lambda}{2-2\lambda}\right) m_h^*. \quad (86)$$

Finally, solution of the group mass $m_g(m_h, a)$ is (from Eq. (72)),

$$m_g = M_h(a) \frac{(1-\lambda)}{\sqrt{\pi\eta_0}} \left(\frac{m_h^*}{m_h}\right)^\lambda \frac{m_p}{m_h^*} \exp\left[-\frac{1}{4\eta_0} \left(\frac{m_h}{m_h^*}\right)^{2-2\lambda}\right]. \quad (87)$$

The mass flux and transfer functions can be obtained from definitions (Eqs. (15), (18)) in Section 4.1, where the mass transfer function is

$$T_m = \frac{1-\lambda}{2\eta_0\sqrt{\pi\eta_0}} \frac{1}{\tau_h^*(a)} \left(\frac{m_h}{m_h^*}\right)^{2-3\lambda} \exp\left[-\frac{1}{4\eta_0} \left(\frac{m_h}{m_h^*}\right)^{2-2\lambda}\right]. \quad (88)$$

Here $T_m(m_h, a) \propto m_g(m_h/m_p)^{2-2\lambda}$ is a typical feature of heterogeneous diffusion. The mass flux function is finally given by,

$$\begin{aligned} \Pi_m(m_h, a) = -\frac{m_h^*(a)}{\tau_h^*(a)} \left\{ \underbrace{\text{erfc}\left[\frac{1}{2\sqrt{\eta_0}} \left(\frac{m_h}{m_h^*}\right)^{1-\lambda}\right]}_I \right. \\ \left. + \underbrace{\frac{1}{\sqrt{\eta_0\pi}} \left(\frac{m_h}{m_h^*}\right)^{1-\lambda} \exp\left[-\frac{1}{4\eta_0} \left(\frac{m_h}{m_h^*}\right)^{2-2\lambda}\right]}_{II} \right\}, \end{aligned} \quad (89)$$

with term I (complementary error function) dominates for small m_h and term II (exponential function) dominates for large m_h . Additionally, $\Pi_m(m_h, a) = \varepsilon_m$ with $m_h \rightarrow 0$ satisfies the boundary conditions (Eq. (76)).

Figure 9 plots the variation of the halo mass function f_M (Eq. (80)), mass transfer function $-\Pi_m$ (Eq. (89)) and mass flux function T_m (Eq. (88)) with halo size n_p for a given set of parameters at the present time t_0 . Two distinct ranges can be clearly identified from Fig. 9: the mass propagation range with a constant mass flux $\varepsilon_m = \Pi_m$ for $m_h < m_h^*$ and mass deposition range for $m_h > m_h^*$.

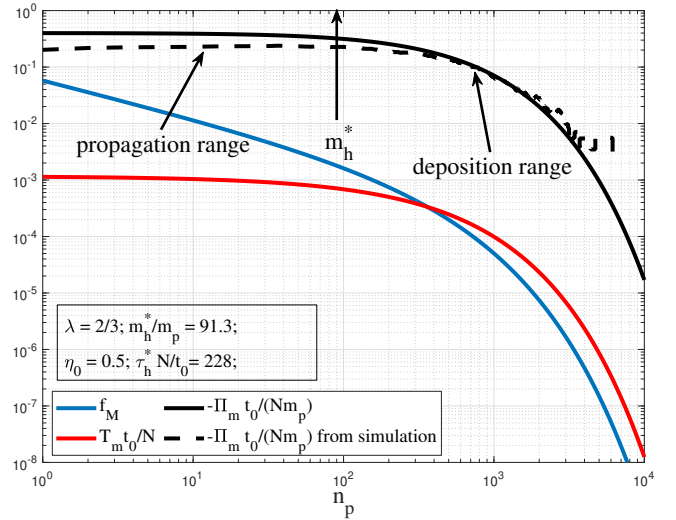


Figure 9. The variation of halo mass function f_M (Eq. (80)), mass transfer function Π_m (Eq. (89)) and mass flux function T_m (Eq. (88)) with halo size $n_p = m_h/m_p$ for a given set of parameters at the current physical time t_0 . Two distinct ranges can be clearly identified: a mass propagation range with a constant mass flux $\varepsilon_m = \Pi_m$ for $m_h < m_h^*$ and a mass deposition range for $m_h > m_h^*$. For comparison, the mass transfer function Π_m obtained using N-body simulation data at two different redshifts $z = 0$ and $z = 0.1$ is also presented in the same plot as dash line.

Figure 10 presents the evolution of mass flux function $-\Pi_m(m, a)$ with redshift z from simulation data in Section 2. The mass flux $-\Pi_m(m, a)$ can be computed from the halo group mass $m_g(m_h, a)$ at two different redshifts using the definition (Eq. (15), Fig. 6, and m_g in dataset (Xu 2022a)). A scale-independent mass flux $\varepsilon_m(a) < 0$ is clearly identified for halo groups smaller than the critical mass $m_h < m_h^*$. The mass propagation range with a scale-independent mass flux $\varepsilon_m(a)$ is formed around $z = 0.3$ and gradually expanding in mass space with increasing time.

5 CONNECTIONS TO HALO MASS FUNCTIONS

5.1 Existing halo mass functions

The abundance of halos, i.e. halo mass function f_M , is one of the most fundamental quantities for analytically or semi-analytically modeling of structure formation and evolution. The Press-Schechter (PS) formalism is one of the first landmark on the halo mass function (Press & Schechter 1974; Bower 1991) that can be used to predict the shape and evolution of the halo mass distribution,

$$\begin{aligned} f_{PS}(m_h) = \frac{1}{\sqrt{2\pi}} \left(1 + \frac{n_{PS}}{3}\right) \frac{1}{m_h} \\ \cdot (m_h/m_h^*)^{\frac{(3+n_{PS})}{6}} \exp\left[-\frac{1}{2} (m_h/m_h^*)^{\frac{(3+n_{PS})}{3}}\right], \end{aligned} \quad (90)$$

where n_{PS} is the effective index of power spectrum of density fluctuation. A normalized dimensionless variable v can be introduced to simplify the halo mass function,

$$v = \frac{\delta_c^2(a)}{\sigma_\delta^2(m_h)} = \left(\frac{m_h}{m_h^*(a)}\right)^{1+\frac{n_{PS}}{3}} = \left[\frac{\sigma_v^2(m_h, a)}{\sigma_v^2(m_h^*)}\right]^{\frac{3+n_{PS}}{3+n}}, \quad (91)$$

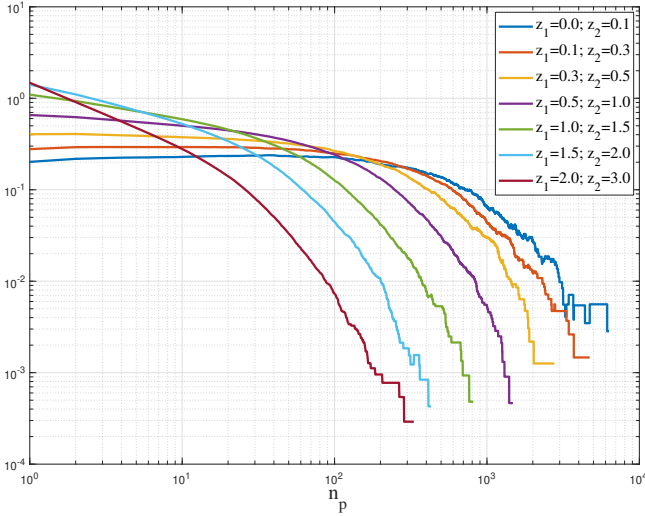


Figure 10. The mass flux function $-\Pi_m(m_h, a)$ (normalized by $N m_p / t_0$) computed from N -body simulations using halo group mass $m_g(a)$ at two different redshifts z (Eq. (15)). A scale-independent mass flux $\varepsilon_m(a)$ can be found for halo groups smaller than the critical mass $m_h < m_h^*$. The negative mass flux $\varepsilon_m(a) = \Pi_m(m_h < m_h^*, a) < 0$ clearly indicates an inverse mass cascade from small to large scales. A mass propagation range (with scale-independent $\varepsilon_m(a)$) is formed at $z = 0.3$ and gradually expands in mass space with decreasing redshift z .

where $\delta_c(a) \sim a^{-1}$ is the critical density that has to be determined from a spherical collapse model or a two-body collapse model (Xu 2021c). Here $\sigma_\delta^2(m_h)$ is the variance of the initial density fluctuation when smoothed with a tophat filter of size $R = (3m_h/4\pi\bar{\rho}_0)^{1/3}$. Here $\bar{\rho}_0$ is the physical background density at the current epoch $a = 1$. The term σ_v^2 is the halo virial velocity dispersion. The second equality in Eq. (91) comes from the linear theory prediction of $\sigma_\delta^2(m_h) \sim m_h^{-(1+n_{ps}/3)}$ for a power-law power spectrum with an effective index of n_{ps} . The third equality in Eq. (91) comes from the virial theorem for halos of mass m_h . Here $\sigma_v^2(m_h) \propto G m_h / r_h^{-n} \propto m_h^{1+n/3}$. The parameter n is the exponent of gravitational potential $V_p(r) \sim r^n$. Since $\delta_c(a) \sim a^{-1}$ from the spherical collapse model, linear theory predicts that $\sigma_v^2(m_h, a) \sim a^{-1} m_h^{1+n_{ps}/3}$, $\sigma_v^2(m_h^*) \sim a$, $m_h^* \sim a^{6/(3+n_{ps})}$ and $v \sim a^{-2} m_h^{1+n_{ps}/3}$.

With the dimensionless variable v introduced in Eq. (91), the equivalent dimensionless form of PS mass function in Eq. (90) is

$$f_{PS}(v) = \frac{1}{\sqrt{2\pi}} v^{-1/2} \exp\left(-\frac{v}{2}\right). \quad (92)$$

Further improvement was achieved by extending the PS formalism with the elliptical collapse model (Sheth et al. 2001; Sheth & Tormen 1999). The modified PS model (ST model, hereafter ST) reads:

$$f_{ST}(v) = \frac{(1 + 1/(qv)^P) \sqrt{2q}}{\Gamma(1/2) + 2^{-P}\Gamma(1/2 - p)} \frac{1}{2\sqrt{v}} e^{-qv/2}. \quad (93)$$

The best fitted parameters from large-scale N -body simulations is $q = 0.75$ and $p = 0.3$ (Sheth & Tormen 2002). Many other forms of empirical mass functions were also proposed by fitting to the high-resolution simulation data. For example, a universal JK mass function was proposed to cover a wide range of simulation data with

different cosmologies and redshifts (Jenkins et al. 2001),

$$f_{JK}(v) = \frac{0.315}{2v} \exp\left[-\left|\ln(\sqrt{v}/\delta_c) + 0.61\right|^{3.8}\right]. \quad (94)$$

With $\delta_c = 1.6865$ at $z = 0$. It should be noted that empirical mass function does not satisfy the normalization constraint (Integration of mass function in mass space should give unity) and cannot extrapolate beyond the range of fitting data.

Now let us return to our halo mass function from inverse mass cascade (Eq. (80)), which does not rely on any particular collapse model (spherical or elliptical). If we introduce $v = (m_h/m_h^*)^{2-2\lambda}$, the halo mass function Eq. (80) can be simplified to

$$f_v(v) = \frac{1}{2\sqrt{\pi}\eta_0} v^{-1/2} \exp\left[-\frac{v}{4\eta_0}\right]. \quad (95)$$

Clearly, Eq. (80) reduces to the Press-Schechter (PS) mass function if $\lambda = (3 - n_{ps})/6$ and $\eta_0 = 1/2$ (See Eqs. (91) and (92)). However, it should be noted that Eq. (80) is more general and the parameter η_0 is related to the parameter β_0 (Eq. (82)), where β_0 is the prefactor for power-law scaling in Eq. (24). The halo geometry exponent λ has a fundamental connection to the effective index of power spectrum n_{ps} . In principle, the halo geometry exponent λ should be smaller than 1 such that $n_{ps} > -3$. The effective spectrum index n_{ps} can also be related to the halo fractal dimension as $n_{ps} = 3 - 2D_h$.

A universal halo mass function like Eqs. (92) or (95) is clearly a manifestation of the establishment of intermediate statistically steady state. All these results provide insights into a fundamental question: how the non-equilibrium system maximizes its entropy and approaches the limiting equilibrium via a chain-reaction-like approach and cascade process. Two typical examples are, of course, the hydrodynamic turbulence and SG-CFD (self-gravitating collisionless dark matter flow). Both examples exhibit an intermediate and statistically steady state where a direct energy (or inverse mass & energy) cascade process is well established (Fig. 1).

5.2 Double- λ halo mass function

Both PS and present formulation arrive at a similar form of halo mass function. However, the current formulation of mass function takes an entirely different path based on a fundamental ideas of inverse mass cascade. It can be qualitatively described by a chain reaction model and quantitatively modeled by random walk and heterogeneous diffusion model. The critical overdensity δ_c from spherical or elliptical collapse model is not required in this formulation.

Since the halo geometry parameter λ can be slightly dependent on mass scale and varying within range of $[2/3, 1]$, the mass function we derived (Eq. (80)) can be naturally generalized to a double- λ mass function with two different values of λ for the propagation range (power-law with λ_1) and deposition range (exponential with λ_2), respectively. Based on this idea, a double- λ mass function is proposed from Eq. (80),

$$f_M(m_h, a) = (2\sqrt{\eta_0})^{-q} \frac{2(1-\lambda_1)}{q\Gamma(q/2)} \cdot \frac{(m_h^*/m_h)^{\lambda_1}}{m_h^*} \exp\left[-\frac{1}{4\eta_0} (m_h/m_h^*)^{2-2\lambda_2}\right], \quad (96)$$

where $q = (1 - \lambda_1)/(1 - \lambda_2)$ is the ratio between two λ values to satisfy normalization constraint. The k th order moments of the

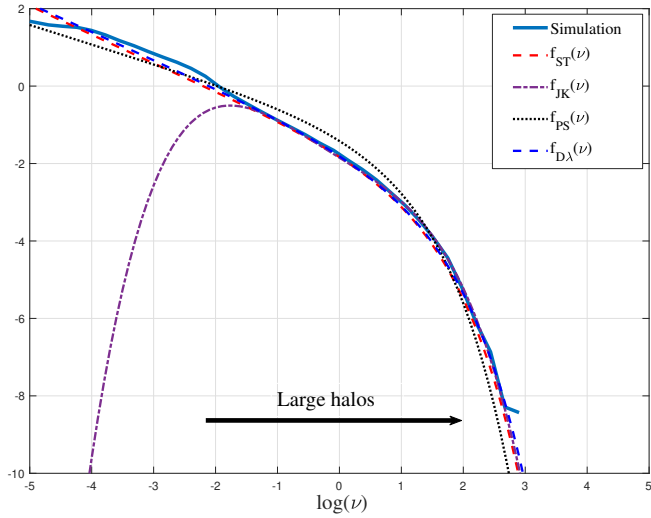


Figure 11. Comparison between different mass functions ($\log(f(v))$) and simulation data at $z=0$. The PS mass function underestimates the mass in large halos. The fitted JK mass function matches simulation for a given range of halo size, but not entire range. The double- λ mass function (Eq. (98)) matches both simulation and ST mass function for entire range.

double- λ mass function is

$$\int_0^\infty f_M(m_h, a) (m_h)^k dm_h = \frac{q/2}{\Gamma(1+q/2)} (4\eta_0)^{\frac{k}{(2-2\lambda_2)}} \Gamma\left(\frac{q}{2} + \frac{k}{2-2\lambda_2}\right) (m_h^*)^k. \quad (97)$$

With the dimensionless variable defined as $v = (m_h/m_h^*)^{2-2\lambda_2}$, the double- λ mass function can be conveniently transformed to dimensionless form,

$$f_{D\lambda}(v) = \frac{(2\sqrt{\eta_0})^{-q}}{\Gamma(q/2)} v^{q/2-1} \exp\left(-\frac{v}{4\eta_0}\right). \quad (98)$$

The best fit to the simulation data gives values of $\eta_0 = 0.76$ and $q = 0.556$. With $\lambda_2 = 2/3$ for the deposition range, it can be estimated that $\lambda_1 = 0.815$ for propagation range. This idea can be even extended to a more general mass function with λ continuously varying with mass to allow the best fit to simulation data.

Figure 11 plots different dimensionless mass functions ($\log(f(v))$) compared with the simulation data described in Section 2. The PS mass function underestimates the mass in large halos. The fitted JK mass function matches the simulation only for a given range of halo mass. The double- λ mass function matches both the simulation and ST mass function for the entire range.

6 CONCLUSIONS

By revisiting fundamental ideas of hydrodynamic turbulence, the mass cascade of self-gravitating collisionless fluid dynamics (SG-CFD) shares many similarities with the energy cascade of a two-dimensional turbulence. This paper reformulates SG-CFD (dark matter flow) to explore new discoveries and insights. We specifically focus on the inverse mass cascade among groups of halos and its direct effects on halo mass functions.

This is a very important and huge topic for structure formation and evolution. It begins with a halo-based description of large-scale

structures and partition of halos into groups of same mass. The mass redistribution among halo groups is described by redistribution functions at different redshifts (Eqs. (1) and (2)). The mass cascade is shown to be local, two-way, and asymmetric in halo mass space (Figs. 3, 4, and 5). Halos inherit/pass their mass mostly from/to halos of the same or similar sizes. The net mass transfer is upward that proceeds in a “bottom-up” fashion. Two distinct ranges are identified for the inverse mass cascade based on a simple analysis of relevant time/mass scales (Eqs. (4), (6), (7) and (8)), i.e. a mass propagation range with a scale-independent rate of mass transfer below a characteristic mass m_h^* and a mass deposition range where mass cascaded from small scales is actively consumed to grow halos (Figs. 8 and 9).

These ideas are further developed by introducing the mass flux and mass transfer functions (Eqs. (15) and (18)). Simple dimensional analysis leads to a power-law mass function for mass propagation range with an exponent λ related to the halo geometry (Eq. (24)). A fundamental merging frequency $f_0(m_p, a) \sim m_p^{\lambda-1} a^{-\tau_0}$ is found with $\tau_0 = 1$ expected. The scaling with scale factor a is the same as the cosmological redshift of photon frequency. The particle mass can be determined if the frequency f_0 can be measured and known. The rate of mass injected into halo sub-system at the smallest scale decreases with a as $\epsilon_m(a) \sim a^{-\tau_0}$ (Eq. (39)). The mean waiting time or the lifespan of halos is shown to scale with halo mass $\tau_g \sim m_h^{-\lambda} a^{\tau_0}$ (Eq. (45)), with $\lambda = 2/3$ expected for large halos. Typical halos grow as $m_h^L \sim a^{3/2}$ with waiting time exactly equal τ_g for every single merging event (Eq. (9)). The mass flux function ϵ_m can be directly related to the rate of mass change of a typical halo m_h^L (Eq. (54)).

Halo interactions are local in mass space such that a chain reaction model can be used to describe inverse mass cascade as a sequence of mass accretion (Fig. 8). This provides SG-CFD (dark matter flow as a paradigmatic example of non-equilibrium system) a potential mechanism for continuous energy releasing and entropy maximizing. In order to sustain the inverse mass cascade such that total mass in all halos increases as $M_h \sim a^{1/2}$ (Eq. (42)), a continuous injection of mass (“free radicals”) at the smallest scale is required to balance the grow of halo sub-system. To generate these “free radicals”, we postulate either a direct cascade process from large to small scales or a direct generation of “free radicals” at the smallest scale. “Free radicals” should be generated at the same rate as they are consumed and injected into the halo sub-system, i.e. the mass production rate ϵ_m .

Based on the chain reaction description, the inverse mass cascade can be formulated in terms of random walk of halos in mass space (Eq. (68)). Halos are randomly moving in mass space due to mass cascade with an exponential distribution of waiting time (Eq. (63)). This results in a heterogeneous diffusion model with a position-dependent diffusivity (Eq. (77)), where mass function and mass flux/transfer functions can all be analytically derived for the entire range of mass cascade without resorting to spherical or elliptical collapse model (Fig. 9, Eqs. (88) and (89)). Especially, a double- λ mass function (Eq. (96) and (98)) is proposed with two different values of λ for mass propagation and deposition ranges, respectively. Results are compared with simulations and existing mass functions with good agreement (Fig. 11).

In short, the inverse mass cascade is a fundamental feature of the self-gravitating collisionless dark matter flow. A complete understanding of inverse mass cascade and its effects on the structure formation and evolution remains an important and huge topic that requires further study. Some examples of future work are briefly discussed here. Most results presented here are for mass cascade in real space and based on the matter-dominant Einstein-de Sitter (Ed’S) model. Similar analysis can be extended to other cosmological mod-

els. In addition, the mass and energy cascade in Fourier space and energy cascade in real space should be further explored. The effect of mass cascade on density correlation and power spectrum should be investigated. Especially, the non-Gaussian feature developed at small scales from an initially Gaussian density field is highly expected to be an important signature of inverse mass cascade. The mass production rate ε_m should directly impact these non-Gaussian features.

Continuous generation of free radicals at the smallest scale is required to sustain a statistically steady inverse mass cascade. This idea mimics the forced homogeneous isotropic turbulence with a continuous injection of energy at integral scale to balance the energy dissipated at the smallest scale. More work is required on the potential mechanisms to generate those free radicals, which can be either a direct cascade process from large to small scales or a direct generation at the smallest scale. It seems that the intermediate statistically steady state of mass cascade is established around $z = 0.3\text{--}0.5$ (Fig. 10) and evolves as $\varepsilon_m \sim a^{-1}$ to approach the limiting equilibrium. How ε_m changes for different cosmological models is still unknown. Other possible areas of future research for halo migrating in mass space can be an improved continuous-time random walk (CTRW) theory that may provide more insights (Eq. (64)).

DATA AVAILABILITY

The data underlying this article are available on Zenodo (Xu 2022a,b,c). All data files are also available on GitHub (Xu 2022d).

REFERENCES

- Blumenthal G. R., Faber S. M., Primack J. R., Rees M. J., 1984, *Nature*, 311, 517
- Bond J. R., Cole S., Efstathiou G., Kaiser N., 1991, *Astrophysical Journal*, 379, 440
- Bower R. G., 1991, *Monthly Notices of the Royal Astronomical Society*, 248, 332
- Colberg J. M., White S. D. M., Jenkins A., Pearce F. R., 1999, *Monthly Notices of the Royal Astronomical Society*, 308, 593
- Cooray A., Sheth R., 2002, *Physics Reports-Review Section of Physics Letters*, 372, 1
- Frenk C. S., et al., 2000, arXiv:astro-ph/0007362v1
- Gunn J. E., Gott J. R., 1972, *Astrophysical Journal*, 176, 1
- Jenkins A., et al., 1998, *Astrophysical Journal*, 499, 20
- Jenkins A., Frenk C. S., White S. D. M., Colberg J. M., Cole S., Evrard A. E., Couchman H. M. P., Yoshida N., 2001, *Monthly Notices of the Royal Astronomical Society*, 321, 372
- Kraichnan R. H., 1967, *Physics of Fluids*, 10, 1417
- Lukic Z., Heitmann K., Habib S., Bashinsky S., Ricker P. M., 2007, *Astrophysical Journal*, 671, 1160
- McBride J., Fakhouri O., Ma C. P., 2009, *Monthly Notices of the Royal Astronomical Society*, 398, 1858
- Neyman J., Scott E. L., 1952, *Astrophysical Journal*, 116, 144
- Press W. H., Schechter P., 1974, *Astrophysical Journal*, 187, 425
- Richardson L. F., 1922, *Weather Prediction by Numerical Process*. Cambridge University Press, Cambridge, UK
- Sheth R. K., Tormen G., 1999, *Monthly Notices of the Royal Astronomical Society*, 308, 119
- Sheth R. K., Tormen G., 2002, *Monthly Notices of the Royal Astronomical Society*, 329, 61
- Sheth R. K., Mo H. J., Tormen G., 2001, *Monthly Notices of the Royal Astronomical Society*, 323, 1
- Stratonovich R. L., 1966, *SIAM Journal on Control*, 4, 362–371
- Tomita K., 1969, *Progress of Theoretical Physics*, 42, 9
- Xu Z., 2021a, arXiv e-prints, p. arXiv:2109.12244
- Xu Z., 2021b, arXiv e-prints, p. arXiv:2110.03126
- Xu Z., 2021c, arXiv e-prints, p. arXiv:2110.05784
- Xu Z., 2021d, arXiv e-prints, p. arXiv:2110.09676
- Xu Z., 2021e, arXiv e-prints, p. arXiv:2110.13885
- Xu Z., 2022c, A comparative study of dark matter flow & hydrodynamic turbulence and its applications, doi:10.5281/zenodo.6569901, <http://dx.doi.org/10.5281/zenodo.6569901>
- Xu Z., 2022d, Dark matter flow dataset, doi:10.5281/zenodo.6586212, https://github.com/ZhiJieXu2022/dark_matter_flow_dataset
- Xu Z., 2022a, Dark matter flow dataset Part I: Halo-based statistics from cosmological N-body simulation, doi:10.5281/zenodo.6541230, <http://dx.doi.org/10.5281/zenodo.6541230>
- Xu Z., 2022b, Dark matter flow dataset Part II: Correlation-based statistics from cosmological N-body simulation, doi:10.5281/zenodo.6569898, <http://dx.doi.org/10.5281/zenodo.6569898>
- Xu Z., 2022e, arXiv e-prints, p. arXiv:2201.12665
- Xu Z., 2022f, arXiv e-prints, p. arXiv:2202.00910
- Xu Z., 2022g, arXiv e-prints, p. arXiv:2202.02991
- Xu Z., 2022h, arXiv e-prints, p. arXiv:2202.04054
- Xu Z., 2022i, arXiv e-prints, p. arXiv:2202.06515
- Xu Z., 2022j, arXiv e-prints, p. arXiv:2202.07240
- Xu Z., 2022k, arXiv e-prints, p. arXiv:2203.05606
- Xu Z., 2022l, arXiv e-prints, p. arXiv:2203.06899